Stratigraphy as a low-pass filter: selective preservation of spatial variability on a Holocene carbonate platform

Xianyi Liu[1*], Sam J. Purkis[2], Peter Burgess[3], David De Vleeschouwer[4], Laurent Puyana[2], Niklas Hohmann[1], Emilia Jarochowska[1]

1 Department of Earth Sciences, Utrecht University, Vening Meinesz building A, Princetonlaan 8a, 3584 CB Utrecht, The Netherlands

2 Department of Marine Geosciences, University of Miami, 4600 Rickenbacker Causeway Miami, FL 33149-103, USA

3 Department of Earth, Ocean and Ecological Science, University of Liverpool, Brownlow St, Liverpool L69 5GP, United Kingdom

4 Institut für Geologie und Paläontologie, Universität Münster, Corrensstr. 24, 48149 Münster, Germany

*Email address: x.liu6@uu.nl;

Abstract: Walther's law, a fundamental principle in geoscience, predicts that laterally adjacent depositional environments become preserved as a vertical succession of layers (facies). As an expression of uniformitarianism, this law underpins interpretations of Earth's history, yet it has not been quantitatively tested. We test this law and examine its limitations by quantifying multidecadal changes in environmental heterogeneity (1945-2019) in the Bahamas and extrapolating them to millennial timescales using forward modelling. Virtual stratigraphic successions predicted by Walther's law contain substantially greater heterogeneity than observed in sediment cores. This discrepancy arises because small and short-lived environment patches undergo rapid turnover and fail to accumulate sufficient sediment for preservation. Our work establishes a quantitative framework for defining preservation thresholds and demonstrates that stratigraphy functions as a low-pass filter on environmental variability, selectively preserving low spatial- and temporal-frequency environmental signals. These findings fundamentally constrain how environmental change can be reconstructed from the sedimentary record.

Keywords: The Bahamas, Walther's law, remote sensing, carbonate sedimentology, stratigraphy

Introduction

Sedimentary rocks provide the primary archives of Earth's environmental and evolutionary history, but we lack a quantitative understanding of how they record environmental and ecological variability. Walther's law provides a qualitative framework linking space to geological time (represented by stratigraphy). This law posits that laterally adjacent depositional environments become vertically stacked in the stratigraphic record, provided migrating environmental patches and sufficient time for sediment accumulation. This law has been applied extensively to reconstruct subsurface geobody distributions (*1*), paleo-environments, as well as past ecosystems (*2-4*). Walther's law is an expression of uniformitarianism, an approach assuming that processes observed on the Earth's surface today have applied in its past. It predicts that dynamic spatial heterogeneity will be preserved as stratigraphically complex successions (*5-7*). However, Walther's law and its underlying uniformitarian approach have not been tested through direct observations or experiments, because quantitative data on spatial heterogeneity in modern depositional systems is hardly available over timescales relevant to the formation of stratigraphic records.

In-situ ecological and environmental monitoring typically spans months to a few years, with a median observational duration of only 10 months (*8*), whereas only a handful of studies have reached decadal timescales through the use of multi-proxy archives (*9, 10*). In contrast, geological reconstructions of environmental change integrate signals over millennial or longer timescales and are subject to time averaging and large uncertainties. As a result, observations at multidecadal timescales remain rare, leaving a critical observational gap between modern ecological dynamics and the processes that ultimately generate stratigraphy. The multidecadal timescale represents the essential transition between the transient behavior of environmental patches and the stratigraphic signals preserved in the rock record (*11*), enabling the study of how the spatial heterogeneity observed in modern carbonate systems is retained or lost in stratigraphy.

Given their highly heterogeneous and dynamic nature, shallow-marine carbonate platforms are a natural laboratory for testing Walther's law. Tropical carbonate platforms are ecosystems composed of a range of shallow-marine benthic habitats, including coral reefs, seagrass meadows, tidal flats and channels. These habitats are spatially heterogeneous and dynamically evolving, reflecting their sensitivity to external drivers such as climate, sea level, storms, and hydrodynamics, as well as internal biotic interactions including competition, facilitation, and dispersal (*12-14*). Habitat heterogeneity is interesting from both ecological and geological perspectives. For ecologists, habitat distribution and its temporal evolution underpin biodiversity (*15, 16*) and ecological stability (*17*). For geologists, carbonate producers are typically associated with specific habitats (*18*), such that habitat shifts influence carbonate production rates and composition, thus directly affecting the formation of

distinct types of sediments and organism remains, collectively termed “facies” (*19, 20*). Determining how these habitats change through time can help us bridge short-term processes and long-term geological histories.

In this study, we quantify how environmental heterogeneity is transferred from modern depositional environments into the geological record by reconstructing changes in benthic shallow-water habitat distributions in the Bahamas between 1945 and 2019 using vintage aerial photos and modern satellite imagery in the Bahamas. We focus on the North Abacos and the Joulters Cays, two areas with contrasting depositional and hydrodynamic regimes, and quantify changes in spatial heterogeneity and habitat patch characteristics over multidecadal timescales in both regions. We combine (1) habitat distribution changes between 1945 and 2019, (2) sediment cores accumulated over multiple millennia, and (3) forward stratigraphic modeling, which translates spatial ecological dynamics into vertical facies successions through the application of Walther’s law. By comparing the three datasets, we examine how spatial heterogeneity would be preserved under an explicit application of Walther’s law. We show that the geological record systematically underrepresents short-lived and small-scale environmental variation, because rapid environmental turnover prevents sediment accumulation that is sufficient for preservation. We propose a framework for quantifying the threshold that an environmental patch must clear in order to become preserved in the sedimentary record. Our results demonstrate that stratigraphy acts as a low-pass filter on environmental variability, preferentially preserving environmental signals that exceed thresholds in temporal persistence and spatial extent. Our findings establish quantitative framework to set limits on the preservation of environmental heterogeneity and provide a mechanistic link between ecological dynamics and the formation of the stratigraphic record.

Geographic background

We chose two well-studied areas from the Bahamas for this study: the Joulters Cays on the Great Bahama Bank and the North Abacos on the Little Bahama Bank (Figure 1). Both areas host similar shallow-marine habitats, but differ in their hydrodynamic and depositional settings, allowing an assessment of habitat dynamics under contrasting environmental conditions.

The Joulters Cays are a crest of islands formed from ooid shoals located in North Andros on the Great Bahama Bank that emerged above the sea level in the last 5000 years and has been used as an analogue for carbonate shoal studies for decades (*21*) (Figure 1). This region represents a tide-dominated carbonate system (*22*), located within an over-filled platform interior (*23*). The area is characterized by extensive ooid sand shoals, tidal channels (E-W direction), and adjacent hardgrounds, with hydrodynamics primarily controlled by tidal currents and, to a lesser extent, winds (easterly) and hurricanes (*24*).

The North Abacos region is situated along the northeastern margin of the Little Bahama Bank and is open to the Atlantic Ocean, resulting in a mixed wave- and tide-dominated regime (*25*). Fringing reefs and barrier islands create an elongated lagoon landward of the platform margin, within which seagrass meadows, sand flats and tidal deltas are developed (*26*). The dominant wind direction is NE to E and tide direction is NE-SE (*27, 28*). Compared to the Joulters Cays, the North Abacos experience higher wave energy and more frequent hurricane impacts, leading to different patterns of sediment redistribution and habitat change (*29*).

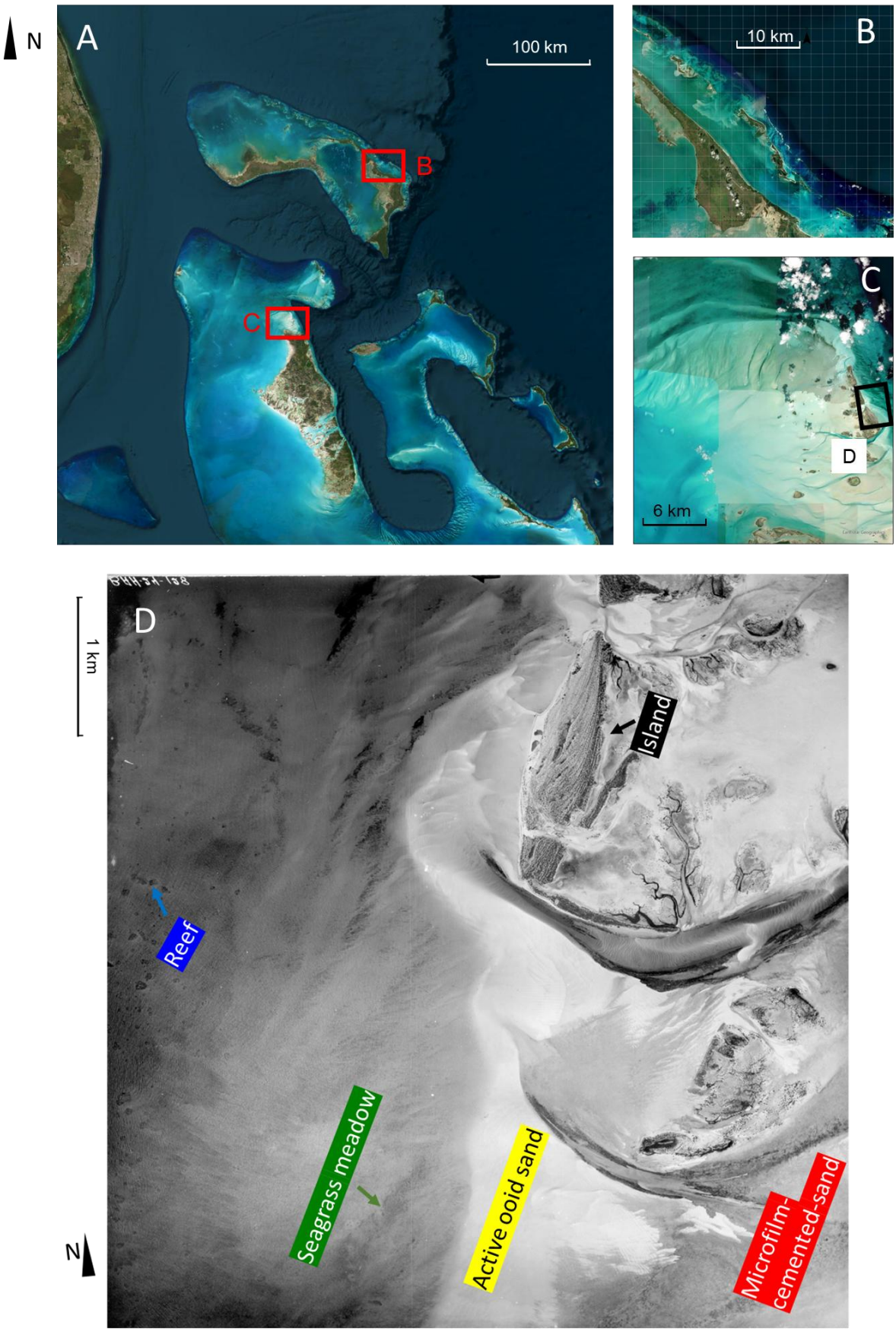
N
A
100 km
B
C
B
10 km
C
D
6 km
D
1 km
Island
Reef
Seagrass meadow
Active ooid sand
Microfilm-cemented-sand
N

Figure 1. A: The satellite image of the Bahamas. B: The North Abacos area. C: The Joulters Cays area. (Copernicus Sentinel data [2025]). D: Example of a digitized vintage photo (BAH-24-128) from the Joulters Cays with interpreted habitat annotations. Images are stored in supplementary Data S1.

Materials and Methods

Materials

Vintage aerial photographs

To compare the decadal-scale habitat transformation, we used aerial photographs acquired in 1945 and stored at RSMAS (Rosenstiel School of Marine, Atmospheric, and Earth Science), University of Miami. These photos were taken using analogue cameras by on-board staff on aircraft and were acquired in the pre-GPS era and, therefore, lack detailed positional metadata. More information about the history of the photographs is provided in previous work (*30*).

The films were developed into 6 in × 6 in grayscale photographs and subsequently scanned with a Canon® CANOSCAN digital scanner at 600 dpi, resulting in an effective spatial resolution of approximately ≤1 m, which is sufficient to resolve benthic features such as patch reefs, seagrass meadows, and sand bodies. This dataset represents one of the earliest spatially extensive records of habitat distribution available for the study areas. The digitized vintage photographs are provided in the supplementary Data S1.

Modern satellite imagery

Modern satellite images were obtained from two sources. The Joulters Cays area was analyzed using SPOT-6 satellite images, whereas the North Abacos region was analyzed using Sentinel-2 imagery. These datasets provide multispectral coverage suitable for distinguishing shallow-marine benthic habitats.

For the North Abacos region, habitat interpretation was validated against an existing benthic facies map published by the Caribbean Natural Conservatory (*31, 32*). Where available, these interpretations were further supported by in-situ sample data.

Method

Processing and Classification

Classification (definition of habitats)

To reduce classification uncertainty, we restrict the analysis to seven broadly defined habitat classes, rather than attempting finer-scale subdivision (Table 1). The following habitat classes are used for surface images: active ooid sand, seagrass meadow, microfilm-cemented sand, macroalgae-cemented sand, hardground, patch reefs, and island. Additionally, the class “slope” was used for areas which are too deep for reasonable interpretation. These classes were selected to represent benthic habitats that are consistently identifiable in both vintage aerial photographs and modern satellite imagery. Not all classes were present in all areas.

The classes reflect visually distinguishable features in the imagery and are defined based on tone, texture, geometry, and spatial context. The diagnostic characteristics used for interpretation are summarized in Table 1.

Table 1. Identification criteria for benthic habitats in vintage images and modern satellite images.

Habitat name	Features
Active ooid sand	High brightness, smooth texture

Seagrass meadow	Dark region filled with small circles with rough and not sharp edges
Microfilm-cemented sand	Intermediate brightness, located in lee side of the ooid active sand
Macroalgae-cemented sand	Intermediate brightness, enclosed geometry, located relatively deep
Hardground	Intermediate brightness, smooth texture, located in the deeper part of the region
Reef	Small enclosed geometry, relatively dark
Island	enclosed shapes bounded by bright ribbon (beach) and filled with dark points (trees), above sea level

Examples of five habitat classes are shown in Figure 1D. Because ground-truth data are not available for 1945, habitat interpretation for the vintage imagery relies on visual criteria and comparison with modern datasets.

Assembling composite images

The digitized vintage photographs were assembled into composite images using Agisoft Metashape®. This software identifies common features among individual overlapping photographs and constructs a composite image. An overlap of ~50% between adjacent photographs is required for successful assembly. More information on the processing workflow and parameter settings are provided in the supplementary text.

The assembled composite images were exported in the TIFF format for subsequent analysis (the JPG version is provided in supplementary Data S2). Two limitations of this approach should be noted. First, the assembled photo loses a certain amount of coverage compared to the coverage provided by the original photos because areas with insufficient overlap cannot be reconstructed. Second, variations in exposure among individual photographs may cause localized shifts in brightness and contrast in the composite images.

Georeferencing

After assembling the composite images, they were georeferenced in ESRI ArcGIS®. This was achieved by manually selecting referencing points to align the vintage composite images with a modern basemap. Reference points were chosen on stable features that were unlikely to have migrated over the last decades, such as buildings and large coral reef structures. Features prone to temporal change, including seagrass patches, island shorelines, sand dunes, and other mobile sedimentary structures, were avoided during point selection. The locations and distribution of the selected reference points are reported in the supplementary Data S3.

Object-based classification approach

The georeferenced images were exported to Trimble eCognition® for object-based classification. An object-based approach was selected to incorporate spatial and geometric information into habitat delineation, rather than relying solely on pixel-based classification (*33, 34*). This approach is commonly used in remote sensing studies of benthic habitats and sedimentary systems.

Image segmentation was performed using the 'multi-resolution' segmentation algorithm implemented in eCognition®. Segmentation parameters were chosen to produce objects larger than the native image

resolution, allowing consistent comparison between datasets of differing spatial resolution. For each habitat class, at least 15 spatially distributed training samples were chosen. Habitat classification was then carried out using machine-learning algorithms to assign class labels to image objects based on their spectral and textural attributes.

The segmentation scale parameter was selected to yield a final effective map resolution of approximately 6-7 m (supplementary text). This choice ensured that habitat maps derived from vintage aerial photographs and modern satellite imagery were directly comparable. Details of the classification algorithms, attributes, and parameter settings are described in the supplementary materials.

The classification results were subsequently exported to ArcGIS® for final manual refinement. This step was used to correct obvious misclassifications and ensure spatial consistency among habitat classes, as no automated classification algorithm achieves 100% accuracy. The interpreted shape files are stored in supplementary Data S4.

Quantification of habitat patch heterogeneity

To quantify changes in habitat spatial structure over the last 8 decades, we applied a set of commonly used metrics to characterize the spatial properties of habitat patches (*14, 35-37*), based on area and perimeter of individual patches (original data of patch size and perimeter of each patch are stored in supplementary S5). Specifically, we calculated the Largest Patch Index (LPI), Number of Patches (NP), Mean Patch Area (MPA), and Edge Density (ED, defined as total patch edge length normalized by area). These metrics capture complementary aspects of patch size, abundance, and shape and are widely applied in landscape and seascape analyses.

In addition, Spatial Entropy (SE) was calculated to quantify the overall spatial heterogeneity of each habitat map (*38*), independent of individual habitat classes. SE provides a single measure of map-level heterogeneity and allows comparison between time slices and study areas. Detailed definitions and calculation procedures for all metrics are provided in the supplementary text.

Together, these metrics were selected to characterize changes in habitat patch structure through time in a consistent and reproducible manner, without introducing assumptions about the underlying ecological or sedimentological processes.

Patch tracking and migration data analysis

To quantify habitat patch migration rates and directions, habitat patch aggregates were tracked between the 1945 and 2019 habitat maps by using the R package *plantTracker* (*39*). Herein, by setting a buffer zone, the package is actually tracking patch aggregates that include multiple spatially very close individual patches. Each patch aggregate was assigned a unique identifier and compared across time slices using spatial overlap criteria.

Patches were considered to represent the same feature if they exhibited overlapping areas between time slices. Tracked patches were exported as GeoJSON files, from which migration distances and directions were calculated based on changes in patch centroid positions. Migration rates therefore represent net displacement over the 80-year interval, rather than continuous movement through time. The overall workflow is illustrated in Figure 3.

Because patch tracking requires spatial overlap between time slices, large and persistent habitat patches were more readily tracked than small or short-lived patches. Consequently, migration analyses focus primarily on larger patches for which reliable tracking was possible. This limitation partly reflects the transient nature of small habitat patches rather than a methodological bias and is considered further in the Discussion.

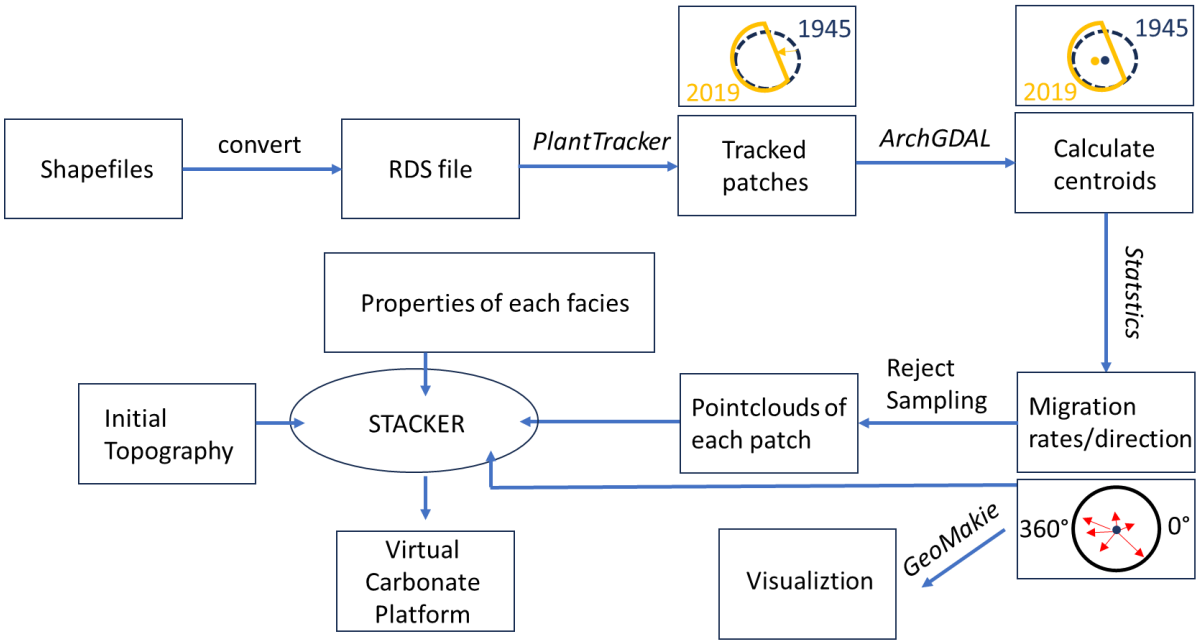

Figure 2. Workflow to process shapefiles from ArcGIS to calculate migration rates and directions of patches, as well as generating cloud points of selected patches. The tracking results (migration of patch centroids) are stored in supplementary Data S6.

Sedimentary cores

Sedimentary cores provide empirical constraints on sediments stacking in both the Joulters Cays and the North Abacos region at geological timescales (Figure 4). Of 60 available sedimentary cores at the Joulters Cays, five cores located along the shoal were selected for comparison (*40*), as they span representative positions across the depositional system. The cores were interpreted based on visual descriptions. The resolution of stratigraphic interpretation is unknown, but we estimate it to be around 5 cm based on the thinnest units reported (*41*). The thinnest facies unit is approximately 9-10 cm thick. Two cores from the North Abacos are selected from a total of 6 marine sediment cores (*42, 43*). Although they are located at the edge of the study area, they still provide the main sedimentological features of this region. Core 'TW' and core 'CR' are located at the lee- and wind- side of the coral barrier, respectively, representing contrasting hydrodynamical settings. These cores are situated near boundaries between island, microfilm-cemented-sand, active ooid sand, and seagrass meadow habitats, and therefore capture variability across key facies transitions (Figure 6).

Geological forward modeling (STACKER)

Direct comparison between 2D spatial heterogeneity in habitat maps with 1D stratigraphic heterogeneity recorded in sediment cores is challenging. To bridge this dimensional gap, we use the carbonate forward model STACKER (*44*) attempting implementing Walther's law by converting lateral habitat migration (patch dynamic patterns) and 2D habitat distribution data into vertical facies stacking. Walther's law has been formulated in a general form and applying it in a forward model requires making assumptions on the accumulation and migration rates of facies covered by this law. Here we follow the uniformitarian approach exemplified by this law and inform modeling scenarios by patch parameters and sediment accumulation rates derived from modern observations. The impact of these assumptions is examined through sensitivity tests, listed in the Supplementary Text. Although multiple forward models exist (*45, 46*), STACKER was selected herein for its conceptual simplicity and suitability for translating mapped habitat migration into stratigraphic architecture.

Each habitat class in the model deposits a distinct facies. For each facies, we assume production rates derived from the literature (Table 2, Supplementary text) (*18*). A single model run can have multiple patches of the same facies, with different shapes, sizes, and migration trajectories derived from patch tracking analysis (Supplementary DataS6). The model additionally requires initial topography (see supplementary Data S7). At each 80-year timestep (for 100 steps, in total 8 kyr), strata accumulate vertically according to assigned production rates within habitat patches migrating laterally with rates and directions specified in one of the test scenarios. Values used in all scenarios follow the uniformitarian approach and are derived from observations of the Joulters Cays. The null scenario (S0), which we consider to represent empirical processes the best, assumed modern median annual sediment production values (*18*). Since model parameters are informed with empirical values, which themselves show great variability, we conducted a series of sensitivity tests to assess the robustness of our modeling results with respect to the choice of parameter values. Sensitivity tests included: S1) the effect of lowering the resolution of detected bed thickness to 5 and 10 cm, S2) using maximum production rates reported for each facies, S3) patch migration rate lowered ten times, S4) patch migration rate and direction depend on the steepest topographic gradient (details in the Supplementary Table S7).

Modelling is limited to the five largest tracked patch aggregates for ooid sand, seagrass meadow, macroalgae, microfilm-cemented sand, and reef, because reliable migration rates could not be derived for smaller and more transient patches (see patch tracking section). However, modelling analysis demonstrates that this does not cause an unrealistic decrease in spatial heterogeneity (Supplementary text).

STACKER does not model erosion, transport, or post-depositional bioturbation or diagenetic modification. The modelled stratigraphic heterogeneity is therefore a simple consequence of observed habitat migration and accumulation rates. Cross-sections (Supplementary text, Fig. S9) and virtual cores extracted from the modeled carbonate platform were compared with observed sediment cores. Because STACKER operates on habitat patches rather than lithologies, modeled facies were converted to observed sedimentary facies using the depositional framework of Harris (*40*) (Table 2).

Table 2. Conversion matrix between habitat classes, facies classes and production rates for facies

Depositional Environment (Harris 1979)	**Description (Harris 1979)**	**Habitat**	**Facies**	**Production rate**
Mobile Fringe	Well sorted, medium-sized ooid grain, <1% mud	Active ooid sand	(Ooidal) grainstone	160 m/Myr
Inner Shelf	Seagrass biota, medium sorting, medium-sized ooid/peloid sand grains, <1% mud, 7% skeletal grains	Seagrass meadow	Ooidal packstone	200 m/Myr
Outer Shelf	Abundant corals, poor sorting, very coarse skeletal grains, <2% mud	Reef	Skeletal grainstone	600 m/Myr
Inner Shelf	Green/brown algae, medium sorting, medium-sized ooid/peloid sand grains, <1% mud, 7% skeleton	Macroalgae-cemented sand	Ooidal packstone	190 m/Myr
Sand Flat	Medium sorting, medium-sized ooid/peloid sand	Microfilm-cemented sand	Packstone	40 m/Myr

grains, >5% mud, 25%
skeletal grains

278

279

Results

Key patterns in the habitat distribution maps

The Joulters Cays

This area was dominated by hardground and (patch) reefs in the eastern, deeper part of the region (Figure 3), whereas active ooid sand and islands were situated in the western, shallower part. The proportions of each habitat in vintage and modern images are visualized in Figure 3. Collectively, active ooid sand (vintage: 43.2%, modern: 32.5%), seagrass meadow (vintage: 22.5%, modern: 35.3%), and hardground (vintage: 19.3%, modern: 11.3%), covered ~80% of the area of the region. The median sizes of seagrass meadow, reef and macroalgae-cemented sand polygons were ~3000, 530, 7700 m^2 in vintage images and ~900, 420, 1550 m^2 in modern images, respectively. They are small compared to the total area (e.g., total seagrass meadow area exceeds 3×10^7 m^2). It is noteworthy that despite a rising body of literature using similar remote sensing approach suggested shrinkage of islands area under sea-level rising context (*47*), the islands of the Joulters Cays expanded by 30% in the last eight decades.

The major changes in habitat distribution is visualized in Figure 3C. The seagrass meadow and microfilm-cemented sand gained ~1.065×10^7 m^2 and ~1.8×10^6 m^2 from active ooid sand, respectively. The increasing area of seagrass meadows and microfilm-cemented sand, along with growing islands (net increase by ~2.2×10^6 m^2), indicates the active ooid sand has been gradually stabilized in the past 8 decades. In addition, hardground has been substantially replaced by seagrass meadow. The increase in seagrass meadow area is mainly the result of expansion of the existing seagrass meadow patches (Figure 3): the seagrass grows both towards the onshore (sand shoals) and offshore directions (hardground). During the expansion processes, smaller patches that previously occupied the inter-dune areas became more connected. Similarly, the growth of island area is also mainly achieved by expansion of existing islands.

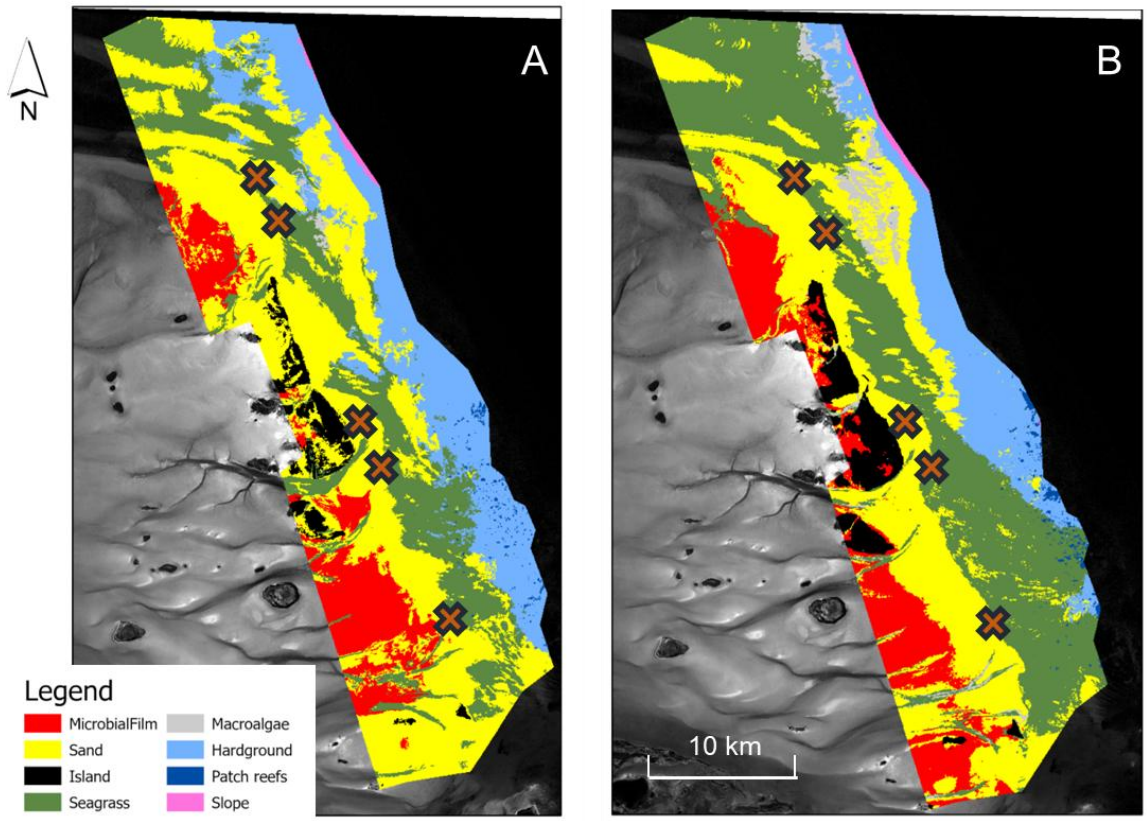
A
B
N
Legend
MicrobialFilm
Sand
Island
Seagrass
Macroalgae
Hardground
Patch reefs
Slope
10 km

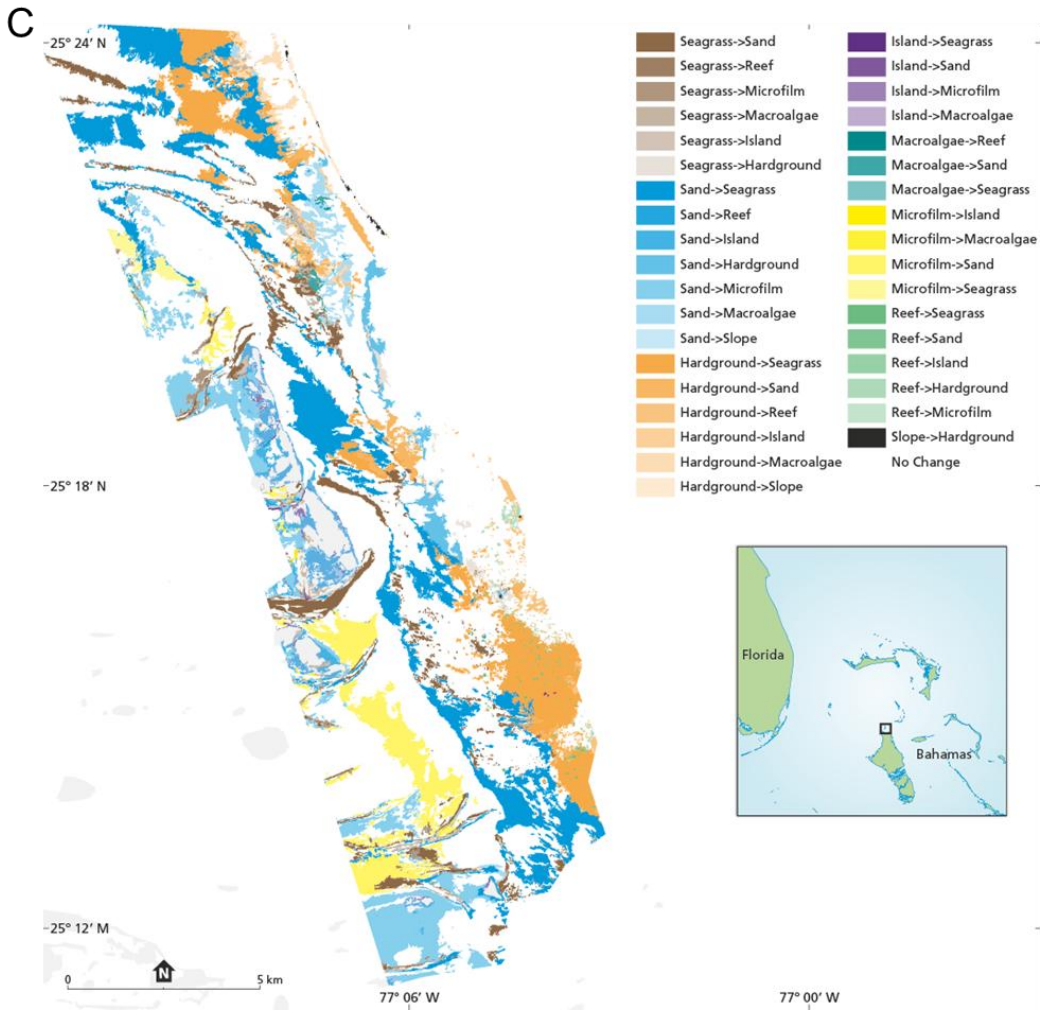
C
25° 24′ N
25° 18′ N
25° 12′ M
0
5 km
77° 06′ W
77° 00′ W
Seagrass->Sand
Seagrass->Reef
Seagrass->Microfilm
Seagrass->Macroalgae
Seagrass->Island
Seagrass->Hardground
Sand->Seagrass
Sand->Reef
Sand->Island
Sand->Hardground
Sand->Microfilm
Sand->Macroalgae
Sand->Slope
Hardground->Seagrass
Hardground->Sand
Hardground->Reef
Hardground->Island
Hardground->Macroalgae
Hardground->Slope
Island->Seagrass
Island->Sand
Island->Microfilm
Island->Macroalgae
Macroalgae->Reef
Macroalgae->Sand
Macroalgae->Seagrass
Microfilm->Island
Microfilm->Macroalgae
Microfilm->Sand
Microfilm->Seagrass
Reef->Seagrass
Reef->Sand
Reef->Island
Reef->Hardground
Reef->Microfilm
Slope->Hardground
No Change
Florida
Bahamas

Figure 3. Interpretation of benthic habitat distribution at the Joulters Cays. A: vintage Vintage (1945) and B: Modern (2019). The cross (black line and orange filling) represents five cores taken for comparison (*40*). Their labels are: "core_78_3_7", "core_78_10_18", "core_78_10_13", "core_78_10_48", "core_2_43", from North to South, respectively. Data is stored in supplementary Data S4. C: Changes in habitat distribution at the Joulters Cays between 1945 and 2019. The base map is from Esri, Tomtom, Garmin, NOAA and USGS.

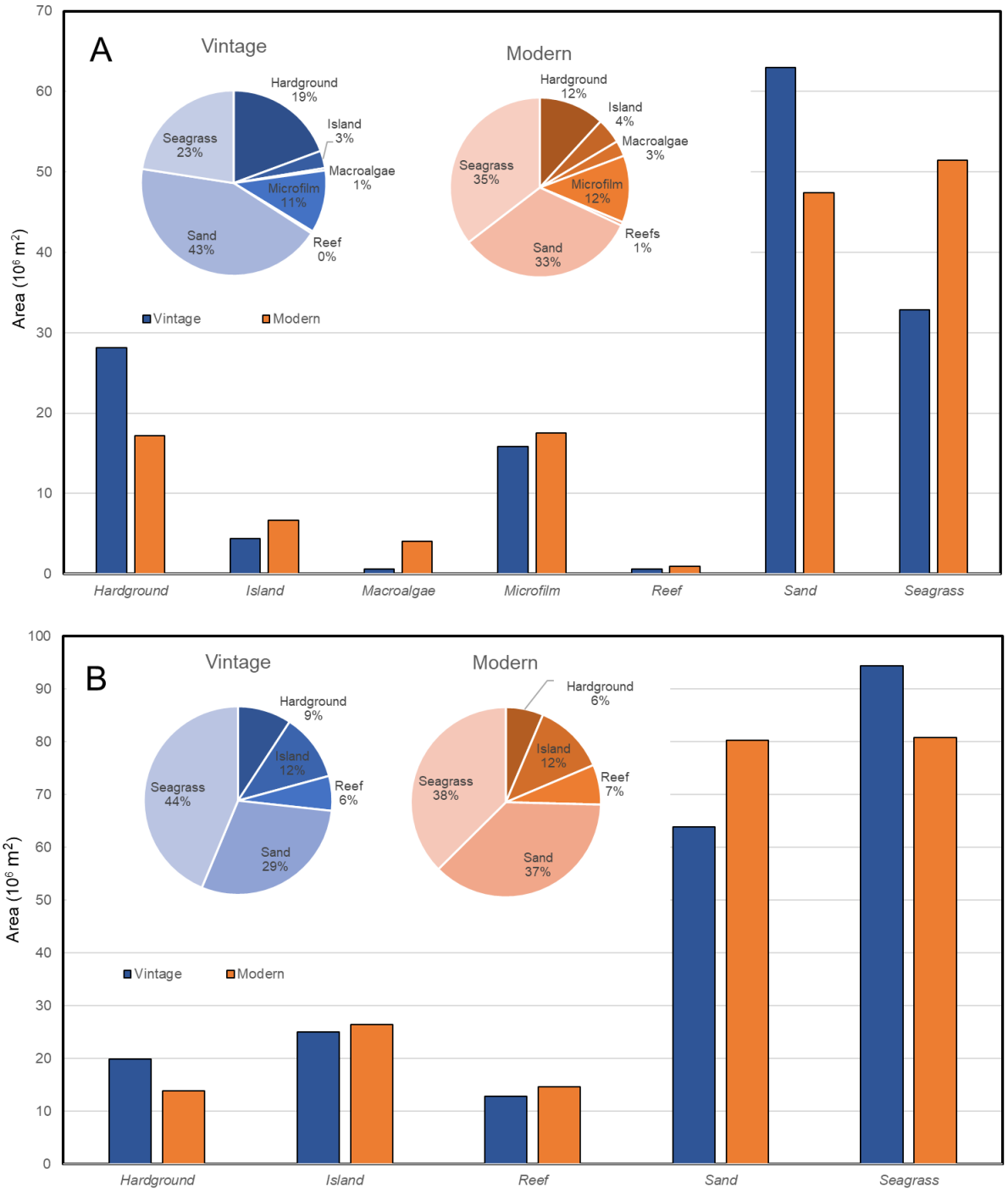

Figure 4. A: Area of each habitat at the Joulters Cays. Small panels indicate proportion of each facies in and in 2019. B: Area of each habitat at the North Abacos. Small panels indicate proportion of each facies in and in 2019. In the pie chart, the area of each slice indicates the proportion of each habitat. Small panels indicate proportion of each facies in and in 2019. Seagrass, microfilm, macroalgae and

sand indicate seagrass meadow, microfilm-cemented-sand, macroalgae-cemented-sand, and active ooid sand, respectively. Raw data of this figure is stored in supplementary S5.

The North Abacos

The North Abacos region was dominated by seagrass meadows (vintage: 43.7%, modern: 37.3%) and active sand (vintage: 29.6%, modern: 37.1%) (Figure 4). Other habitats present included islands, hardground and patch reefs. The major change in this region was nearly opposite to that at the Joulters Cays: seagrass meadows (decrease by ~15%) and hardgrounds (decrease by ~30%) were replaced by active sand. The median sizes of reef patches and seagrass meadows were 212 and 143 m^2 in vintage image, and 3052 and 1127 m^2 in modern image, respectively.

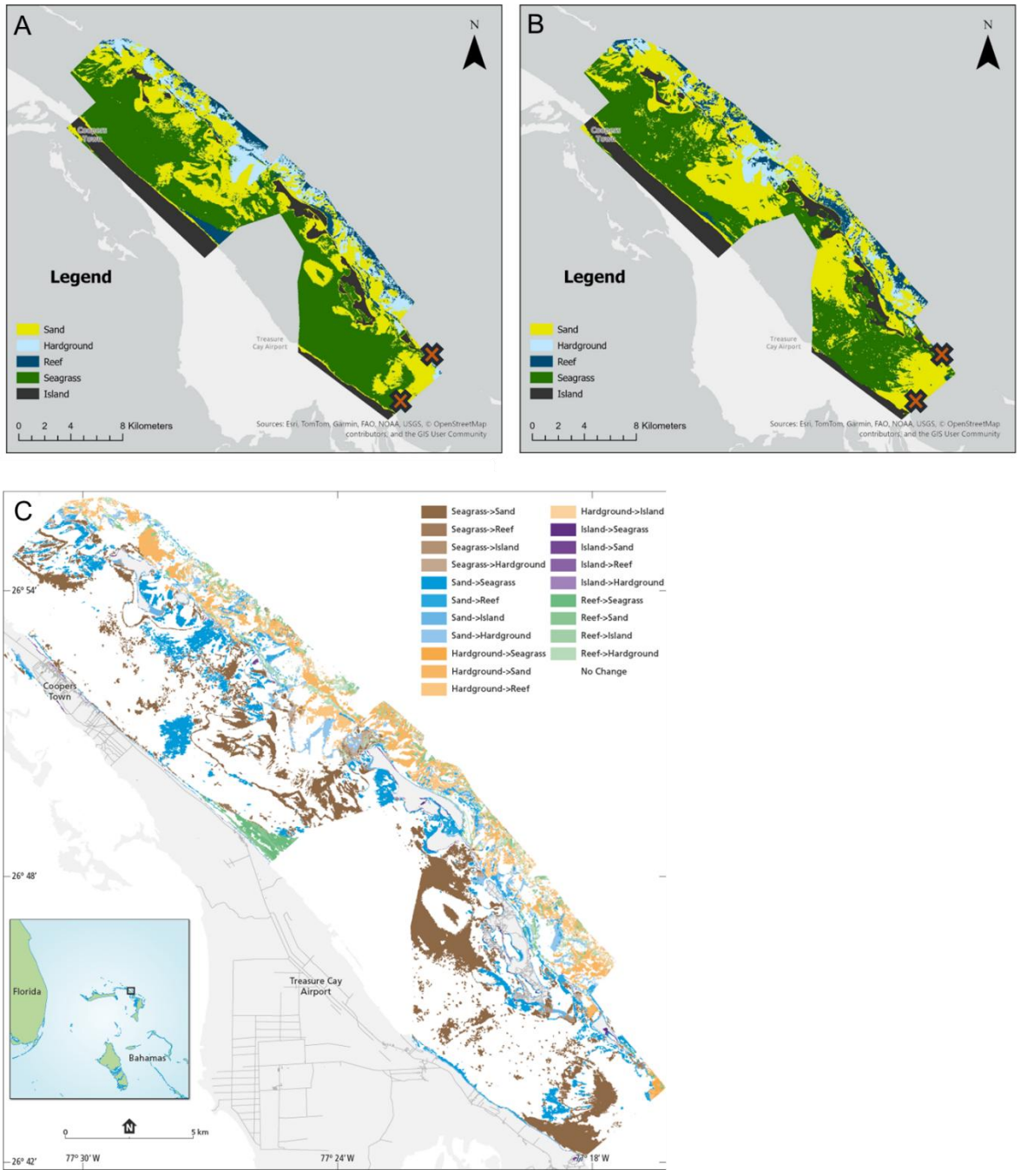

Figure 5. Interpretation of benthic habitat distribution at the North Abacos. A: Vintage (1945) and B: Modern. Two crosses represent the locations of two cores obtained from previous work (*42, 43*): 'TW' – south core, 'CR' – north core. Raw data of this figure is stored in supplementary dataset S4. C:

Changes in habitat distribution in the North Abacos between 1945 and 2019. Base maps are from Esri, Tomtom, Garmin, NOAA and USGS.

The top five changes (in terms of area) in the last 80 years are visualized in Figure 5. Here a completely different story from the Joulters Cays has been observed: we see significant decline in seagrass meadows and hardground areas, and expansion of active ooid sandbars over the last 8 decades. The change map (Figure 5C) indicates that the replacement of seagrass by active ooid sands mainly occurs at the boundaries between seagrass and active ooid sand (i.e., sands expansion), or seagrass patches that were embedded in the active ooid sand. Similarly to the Joulters Cays, the hardground patches have shrunk.

Spatial distribution patterns of habitat patches

The overall SE decreased from 0.054 to 0.038 in the last 8 decades in the Joulters Cays, suggesting a slight decrease in spatial habitat heterogeneity.

Given that seagrass meadows are important habitats in shallow marine ecosystems (*48*) and cover today over 30% of the total area in both Jolters Cays and the North Abacos, we use the seagrass meadow habitat as a case study to show spatial distribution patterns in more detail. The sizes of individual seagrass patches in both areas are summarized in Figure 6. In the study area of seagrass expansion, the Joulters Cays, the distribution of the log-transformed patch area is normal in both time slices. Between 1945 and 2019, smaller patches with sizes between 50 and 10000 m^2 become more abundant. In contrast, in the area experiencing shrinking of seagrass meadows, the North Abacos, the distribution changes from log-normal to bimodal.

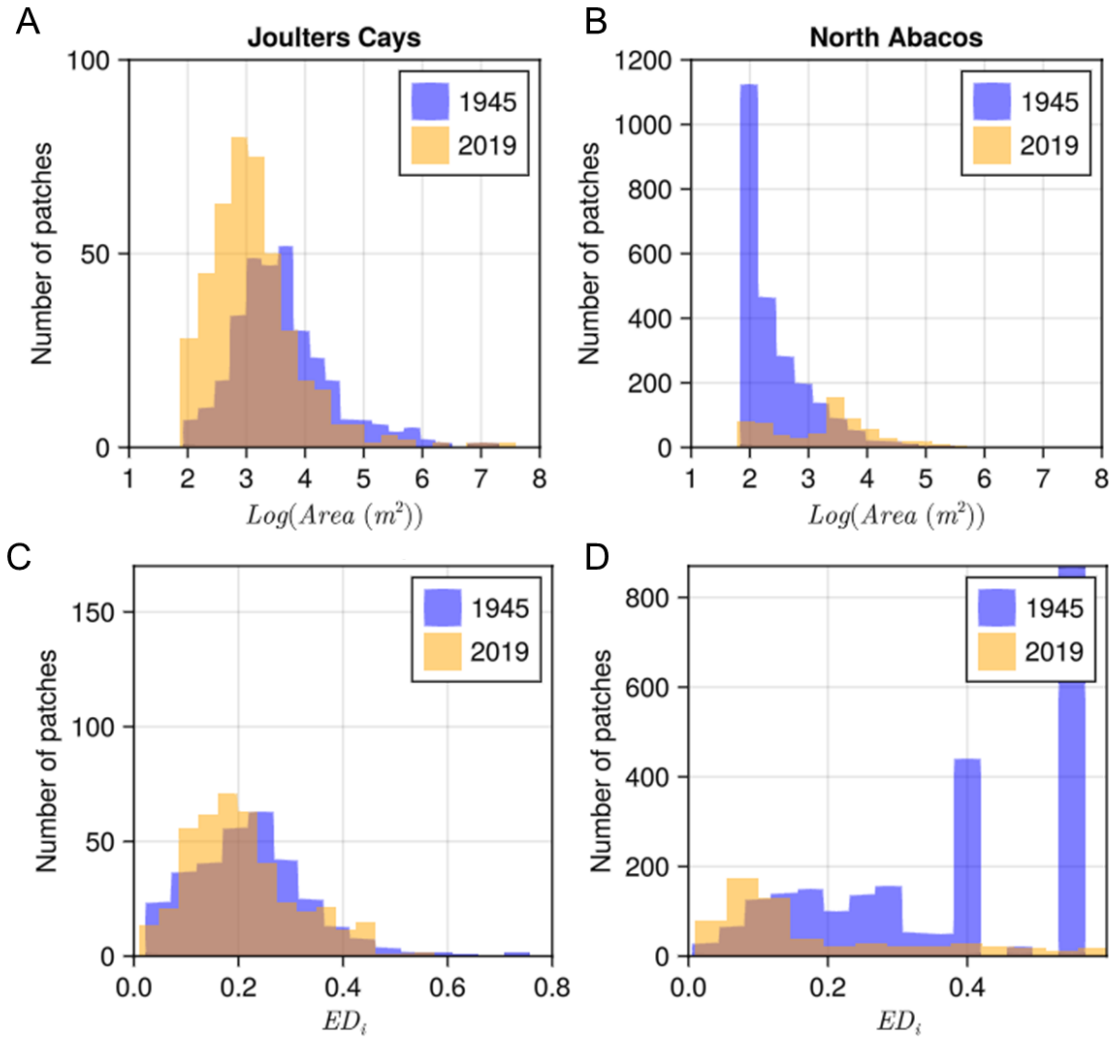

357

358 Figure 6. Distribution of Log_{10}(seagrass meadow patch area) in A: The Joulters Cays; B: The North
359 Abacos; and distribution of ED_i (units: (1/m)) in C: The Joulters Cays; D: The North Abacos; Raw
360 data of this figure is stored in Supplementary Data S5.

361 Table 3. Spatial heterogeneity metrics of seagrass meadow habitat patches.

Metric (unit)	1945		2019	
	The Joulters Cays	The North Abacos	The Joulters Cays	The North Abacos
LPI (%)	49	93	59	83
MPA (m^2)	4066	232	1285	1876
NP	320	2400	425	649
ED (1/m)	0.0371	0.0086	0.0127	0.0132
SE	0.054	0.0559	0.038	0.0049

362

The NP (number of patches) of seagrass meadow patches increased by 30% (320 to 425) at the Joulters Cays, along with the increase in the total area occupied by this habitat (Figure 6). In contrast, the mean (MPA) patch area decreased by 60%. At the North Abacos, as the total coverage by seagrass meadow decreased, the NP decreased from 2400 to 649, and the MPA slightly. The Edge Density (ED) at the Joulters Cays decreased from 0.0371 to 0.0127, while the values for the North Abacos increased from 0.0086 to 0.0132. The Largest Patch Index (LPI) at the Joulters Cays increased from 49% to 59%, while in the North Abacos decreased from 93% to 83%.

In the seagrass meadow expansion area (the Joulters Cays), the median of the ED_i decreased from 0.218 to just below 0.188 (Figure 6). In the shrinking area (the North Abacos), the median of ED_i from 0.388 to 0.117. Such a decrease is driven by the decrease in the number of patches with high ED_i, and an increase in the number of patches with ED_i around 0.1. In both areas, there is thus a shift towards more compact patches, with lower edge-effects, and the shift is much more pronounced at the North Abacos.

Tracking of patches and migration calculations

The parameters used in the *PlantTracker* package are stored in the supplementary text. Tracking shows that the patch aggregates contain not only large patches, but also numerous attached smaller patches. There are 13 ooid active sand patch aggregates, 20 patches of seagrass meadow, 6 of macroalgae-cemented sand, 11 of microfilm-cemented sand, and 49 of reefs. The detailed tracking results are listed in the supplementary text and Data S3-S8. Overall, all large patch aggregates can be identified across the time slices. However, as tracking requires an overlap between vintage and modern patches, *plantTracker* cannot track most of the smaller isolated patches.

The migration rates for ooid active sands and seagrass meadow patch aggregates are 6 to 640 m (mean = 210 m, n =13) m and 20 to 630 m (mean = 220 m, n =20) per 80 years, respectively. Macroalgae- and microfilm-cemented-sand habitat patches also migrated by ~220 m on average over the same interval (Figure S8, Supplementary Data S6). The migration rates for reefs are low: less than 20 m on average per 80 years. This value may indicate the uncertainties associated with the identification of this habitat or may reflect low dispersal rate and competition levels.

Forward simulation and validation with sediment cores

Three facies were detected in the sedimentary cores from the Joulters Cays and the North Abacos: (ooidal) grainstone, ooidal packstone, and packstone. These facies form few thick units (0.1 to 3 m thick). The cores show limited facies alternations (from 0 to 2 times), except for core_78_3_18 (6 times). Facies units in the cores never reach thicknesses lower than 10 cm (*40*). The timespan that the cores represent is unknown, as no age information is provided. However, nearby cores on the sandflat suggest the sediments are of Holocene age (<12 kyr old).

A cross-section produced by the STACKER model run based on the default (S0) scenario of patch migration distributions from the Joulters Cays is shown in Figure S12. From the cross-section, three virtual cores were selected at 25%, 50% and 75% of its length, because their locations correspond approximately to those of the three chosen sediment cores (core_78_3_7, core_78_10_13, core_2_43). The total thickness of the cores is approximately 1 m (Figure 7C), which is comparable to the sediment cores recovered from the Joulters Cays (0.49 to 5.47 m) (*21, 40*). Given that the modeling timespan is 8 kyr, the net sediment accumulation rate is thus less than 0.125 mm/yr (Figure 7C) and such value is within the accumulation rate range for tropical producers reported by Schlager (*49*). This rate is comparable to the sea-level change rate at kyr-scale, allowing the facies to migrate to the niche (i.e., water depth) according to the sea-level change. In these virtual cores, the ooid grainstone formed thick units and were punctuated by repeated thin units of ooidal packstone. Therefore, the sediment cores have substantially thicker facies units and less frequent facies alternations than the virtual cores.

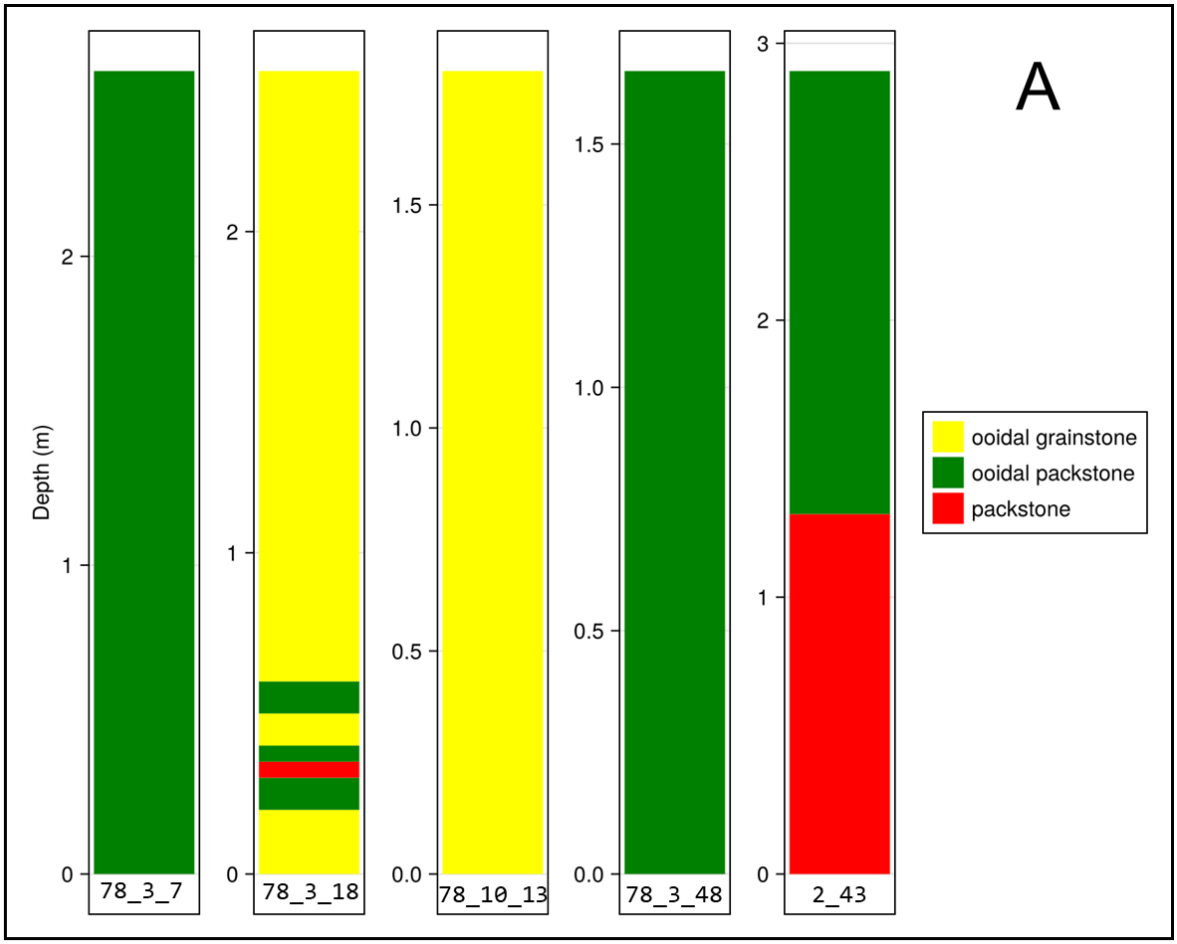
A
Depth (m)
78_3_7
78_3_18
78_10_13
78_3_48
2_43
ooidal grainstone
ooidal packstone
packstone

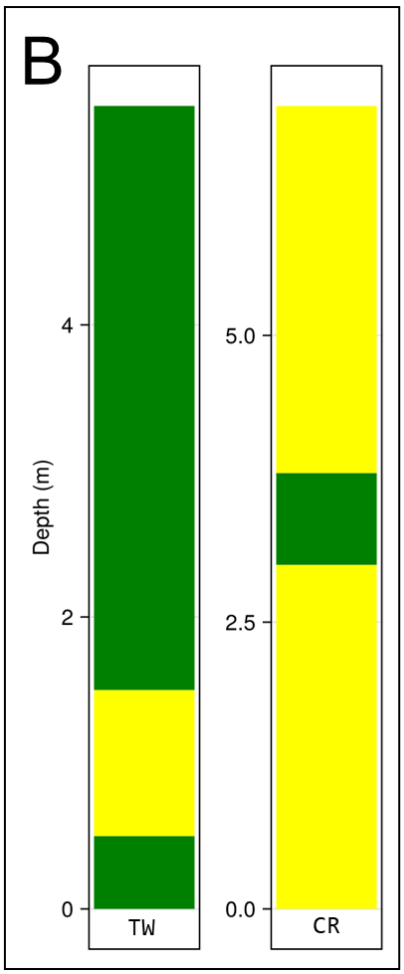
B
Depth (m)
TW
CR

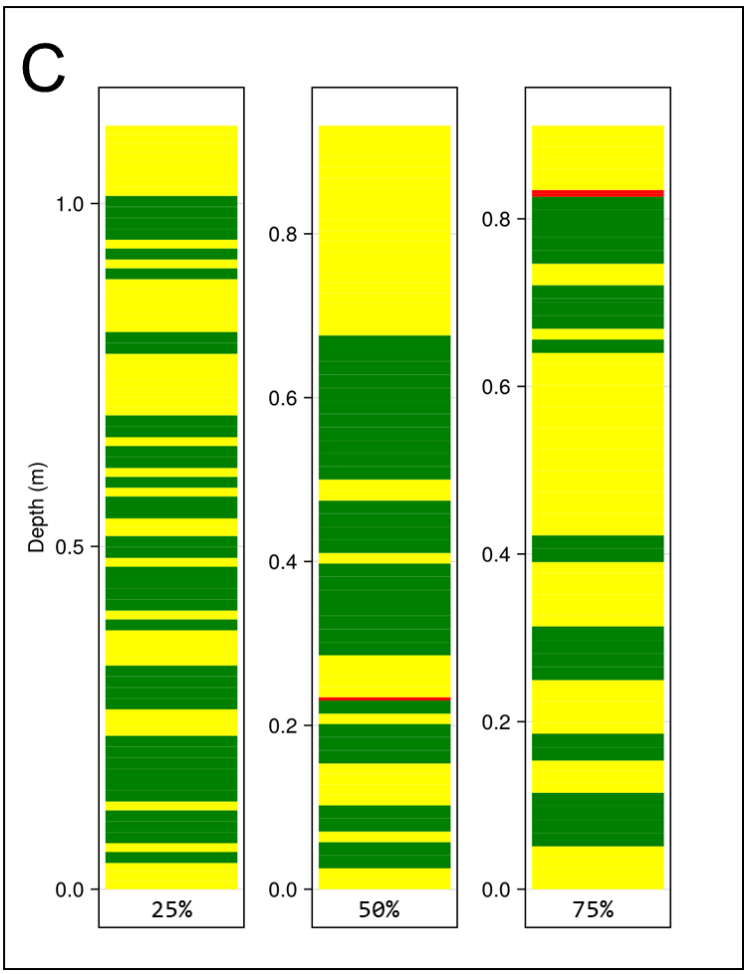
C
Depth (m)
25%
50%
75%

410

Figure 7. Facies distribution in A) Sediment cores at the Joulters Cays, redrawn from Harris (*40*); B) Sediment cores at Treasure Cays, the North Abacos, redrawn from Locker (*42*) and Mullen (*43*); C) Modelling results from the null scenario (S0); data behind panel C is stored in supplementary Data S7 (S0).

To emulate the observational resolution of sedimentary cores, we smoothed the virtual cores with a 5 and 10 cm window (Figure S12A-B). The heterogeneity of the cores has decreased, but multiple facies alternations are still present, despite shorter core thickness than the sedimentary cores.

Discussion

Shallow-marine carbonate habitats in the Bahamas are strikingly dynamic at decadal timescales, yet the stratigraphic record they produce is remarkably homogenous.

Comparing spatial heterogeneities with stratigraphic heterogeneities

Walther's law (*45*) predicts that the dynamic spatially heterogeneous habitat mosaic documented here should translate directly into a stratigraphically complex succession of frequently alternating facies (*14*). The spatial habitat distributions at both sites are dynamic and heterogeneous, comprising at least 5 habitat types and over 1000 individual patches (Figures 3, 5). In contrast, the stratigraphic records from the Joulters Cays and the North Abacos are markedly simple and are characterized by few (in average fewer than 3 per core) facies units (Figure 7). (Ooidal) packstone and ooid grainstone are the dominant facies in the cores. This homogeneity is consistent across datasets: among 60 cores from the Joulters Cays, 55 contain fewer than three facies alternations. Therefore, spatial heterogeneity of the modern habitat mosaic is not transferred faithfully into the stratigraphic record and the transition from spatial habitat variability to vertical facies succession involves a substantial loss of complexity. Considering the stratigraphic succession as a type of signal, we call this effect a ‘low-pass filter’, whereby stratigraphy preferentially preserves ‘low-frequency’ signals, while attenuating ‘high-frequency’ variability.

We used STACKER (*44*), which predicts stratigraphic successions from spatial data, to compare spatial and stratigraphic data quantitatively. While the modelled cores are of similar thickness as the cores from both studied areas in the Bahamas, they contain multiple thin facies units and frequent alternations (Figure 7). Thus, the direct application of Walther’s law by using observed dynamics as modeled by STACKER resulted in more heterogeneous stratigraphy than the empirical sedimentary cores, demonstrating the reduction of heterogeneity during sedimentation processes.

This loss of heterogeneity cannot be explained by how facies classes were discretized in sedimentary cores. In both cases, STACKER as well as the real cores, a limited number of classes had been used, but the granularity of these classes was comparable and followed the standard practice widely used in the Bahamas and other carbonate systems, representative of the level of complexity used in daily stratigraphic practice. Thus, the discretization of spatial data and translation of habitat data into facies cannot be the main mechanism producing the observed complexity reduction.

‘Low-pass-filtering’ effect is present regardless of external forcing

We observed contrasting, complex symbiosis- and competition-like interactions between sand and seagrass patches in the two regions over multi-decadal timescales, and this is consistent with previous studies (*50*). The spatial distribution and dynamics of these habitats are substantially influenced by local external forcing. The large habitat patches are aggregates of smaller connected habitat patches (e.g., Figures 3, 5) displaying a ‘belt-like’ distribution. Such a distribution suggests that water depth is still a crucial factor determining the habitat distribution at the spatial scale of tens of kilometers examined here, in contrast to previous studies (*52*). A mapping of seagrass meadow habitat distribution against water depth (Supplementary text, Figure S13) indicates that seagrass distribution

overlaps with the water depth range between 1 and 3 m, while ooidal sand shoals situated on the shallower shoals (<1 m), and hardgrounds, on the other hand, are located in deeper regions (>3 m).

Sea level is not the only factor controlling habitat distribution. For example, the expansion of seagrass meadows into hardgrounds at the Joulters Cays (~8.5 km^2) may be related to the thin layers of fine-grained sand deposited on the hardground, caused by hurricanes sweeping carbonate sand onto the hardground and providing soft bottom for seagrass growth (*53*). On the other hand, the fringing reefs at the North Abacos act like a barrier that creates a hydrodynamically quiescent lagoon, and the migration of thin fine-grained sand sheets only takes place back and forth on the tidal deltas through a few narrow tidal channels between the barriers (*26*). The migration of tidal deltas can increase the local water turbidity and cover the seagrass meadows, leading to their shrinking.

In spite of the disparate local controls at the Joulters Cays and the North Abacos, the heterogeneity reduction from spatial data to stratigraphic data is observed in both areas. Thus, the 'low-pass-filter' holds across different regions with contrasting settings (e.g., hydrodynamics).

Mechanisms of the 'low-pass-filter'

The reduction in heterogeneity in the transition to the stratigraphic record is a compounded effect of multiple processes. The best studied of them include bioturbation and sediment mixing (*54, 55*). The scale of these processes sets a natural limit to the resolution at which a *waltherian* (i.e. following Walther's law) stratigraphic record forms. In spite of sediment mixing, the sedimentary record is not completely blurred out, it is largely discrete: it consists of individual beds that represent separate facies. This is particularly prominent in tropical carbonates owing to their rapid cementation. Transitions between discrete facies units are routinely interpreted according to Walther's law and such interpretations form the basis of stratigraphy and paleoenvironmental reconstructions. Here we focus on understanding the driving mechanisms of the reduction in heterogeneity specifically how the thinnest facies units are lost in empirical stratigraphic record, resulting in variability loss. For simplicity, we ignore compaction in our reasoning.

Human observational limits on sedimentary cores

We attribute part of the 'low-pass-filter' to the observational resolution in sedimentary cores. Stratigraphic studies rarely report observational resolution explicitly, and in this work we estimated it to be ~5 cm. This observational resolution is further affected by mixing processes, which cause transitions between facies to become gradual (*57*). As we increased the observational window from 1 cm to 5 cm and 10 cm in the virtual cores, the stratigraphic heterogeneity decreased (e.g., from 31 times facies alternating to 17 and 9 times, respectively, in the 25% virtual core) (Figure S10A, B). This reduction primarily reflects the loss of thin beds generated by small and/or short-lived patches (see next section), which amplifies the effectiveness of the 'low-pass-filter'.

Patch persistence and preservation threshold

Operationalizing Walther's law in a stratigraphic forward model allowed us to identify patch properties that determine their fate in the 'low-pass-filter', i.e. achieving a minimum thickness observable in stratigraphy (Equation 1). This equation provides a simple, but useful framework to determine whether an environmental patch is likely to be preserved in the stratigraphy or not.

For a given migration rate, larger patches enable sustained sediment accumulation at a fixed location (i.e., longer duration), leading to the formation of thicker facies units (*38*). For example, assuming a migration rate of 200 m over 80 years, a large circular patch with a radius of 2000 m would require approximately 800 years to move by the distance between its centroid and its edge. Assuming a production rate of 200 m/Myr and applying Equation (1), such a patch would generate ~16 cm of sediment (assuming accumulation rate equal to production rate in this calculation). In contrast, a small patch with a radius of 20 m would produce only ~0.16 cm over the same period. This thickness is far below the minimum thickness of facies units observed in empirical cores (~5 cm) (*40*). Longer

sedimentation time allows for deposition of thicker facies units, which fall above the observational threshold (Supplementary text, sensitivity test S4). Furthermore, smaller patches are more likely to be undersampled in the geological record by sheer chance.

$$Thickness = Duration \times Production\ rate \quad (1)$$

Patch persistence, in combination with production rate, also contributes to the 'low-pass-filter'. The substantial changes in the number of patches (NP) observed over the last 80 years suggest that many patches persist for less than 80 years (i.e., short duration) (Table 3, Figure 6). By employing equation 1 and assuming a production rate of 200 m/Myr for the seagrass meadow habitat (*18*), these patches would generate only 1.6 cm of sediment. This is likewise well below the observational resolution of 5 cm and is therefore unlikely to be resolved (*40*). A patch with this production rate would need to persist for at least ~500 years or exhibit unrealistically high production rates (~1250 m/Myr) to be recorded in sediment cores within 80 years. The low persistence of patches appears in our study to be driven by the 'edge-effect' (ED_i) (*58*). This is because higher edge-effect increases the susceptibility to external influences, reducing patch stability. In both study areas, the number of patches with high ED_i has decreased (Figure 6), suggesting that the patches that are more easily influenced by edge-effects are less persistent in both seagrass expansion and shrinking scenarios (*56*). This result may be in the future validated using neighbor-based approaches to model the dynamics of habitats at decadal timescales (e.g., Cellular Automata) (*59*).

Patch persistence is also strongly linked to patch size (*56*). Tracking results show that large patches persist despite morphological changes over decadal timescales (e.g., the Largest Patch Index, LPI, at the North Abacos decreased from 94% to 83%), whereas small patches frequently appear and disappear in the eight decades timespan. The proportional change in the patch-size distribution (Figure S9) further corroborates this observation and suggests a persistence threshold of approximately 10^3 m^2 over decadal timescales for seagrass meadows. However, defining a threshold relevant to stratigraphic preservation requires observational windows of at least ~500 years, which are not available in the present dataset. Threshold values will vary among habitat types. Together, these results demonstrate that both spatial scale (patch size) and temporal scale (patch persistence) must exceed critical thresholds for sedimentary signals to be resolved.

The mechanism of the 'low-pass-filter' proposed above predicts that 'low frequency' signals,(i.e., habitat patches with larger areas, lower edge-effects (higher compactness) and longer persistence) have higher chances being recorded in stratigraphy.

Other mechanisms

Additional factors affecting the 'low-pass-filter' effect include the following: 1) variations in sediment production rates and the error in their measurement (*60*) (Figure S12C), 2) the period of observation between 1945 and 2019 may not be representative for long-term dynamics and heterogeneity (STACKER section, Supplementary text, Figure S12D, E) and 3) sediment transport (*61, 62*). A simple mass conservation calculation (source-to-sink calculation section, Supplementary text) suggests that a large fraction of sediment produced within habitats is exported. For example, 90% of ooid sands produced in active ooid sand habitats may have been transported onto adjacent islands. This substantial export reduces *in situ* accumulation, further limiting preservation.

Implications for the preservation potential in the stratigraphic record

Stratigraphic records are inherently incomplete, not only due to depositional hiatuses (*63, 64*), but also due to intrinsic 'signal filtering'. As a result, the geological record represents a smoothed archive of past environments.

Our findings do not invalidate Walther's law, but demonstrate its limitations. For example, larger, persistent patches may still be translated into vertical successions as predicted by the law. However, smaller, short-lived patches with higher edge-effects are systematically excluded from the stratigraphic record. This finding has important implications for paleo-environment and paleo-ecological reconstructions based on carbonate depositional systems. Stratigraphic successions likely systematically underestimate the degree of ecological and environmental variability, as 'high frequency' information and dynamics are not preserved during sediment accumulation. As a result, reconstructions based solely on vertical facies successions may oversimplify ancient systems, favoring laterally continuous "belt-like" models over inherently mosaic landscapes (*65, 66*). Our findings also reveal an important limitation of uniformitarianism: modern environmental variability is not preserved uniformly across spatial and temporal scales, requiring scale-dependent interpretation of geological archives.

The filtering effect also impacts cyclostratigraphy. Cyclic facies alternations are commonly used by cyclostratigraphers to identify astronomically forced climate cycles. The underlying assumption is that orbitally driven climate change modulates sea level, causing habitat patches to migrate laterally and generate cyclically alternating facies in the stratigraphic record (*2, 67*). If the low-pass filtering effect described here suppresses the recording of short-lived, small-scale habitat dynamics, the signals that cyclostratigraphers rely upon may be substantially attenuated or even lost entirely (*68*).

Summary

We explored if the extreme spatial and temporal complexity of modern carbonate platforms is reflected in stratigraphy as predicted by Walthers law. We tested this law by combing data from 1) benthic habitat distributions from vintage aerial photographs (1945) and modern satellite imagery (2019) in the Bahamas, 2) sedimentary cores in this region and 3) forward stratigraphic models, and compared the spatial heterogeneity with the stratigraphic heterogeneity.

The two study areas representing different hydrodynamic conditions (the Joulters Cays, the North Abacos) exhibit contrasting decadal trajectories of habitat distributions, with expansion of seagrass meadows at the Joulters Cays and contraction at the North Abacos. In both cases habitat patches with higher edge-effect are less persistent than large patches and undergo frequent appearance, disappearance, merging, and fragmentation.

To assess how such spatial heterogeneity translates into stratigraphy, we used a carbonate forward model (STACKER) to generate virtual stratigraphic successions based on observed habitat migration. When lateral habitat dynamics are translated directly according to Walther's Law, the model predicts frequent vertical alternations of facies. In contrast, real sediment cores from the Joulters Cays record comparatively simple stratigraphic successions dominated by thick, homogeneous facies units.

The mismatch between model predictions and observed sediment cores indicates that stratigraphy preferentially records signals associated with large, persistent habitats, while short-lived, small-scale spatial variability is dampened during sediment accumulation. This selective preservation acts as a stratigraphic low-pass filter, restricting the expression of complex habitat dynamics in vertical facies successions. As a consequence, the direct application of Walther's Law becomes increasingly limited, and this has profound implications for the application of this law and its underlying uniformitarian approach in reconstructing paleo-environment signals from stratigraphy.

Acknowlegements

We thank Garrett Speed (Utrecht University) and Ton Markus (Utrecht University) for advice on GIS, image processing and data management. We also thank Dr. Frits Hilgen (Utrecht University) and Dr. Sietske Batenburg (Utrecht University) for their constructive advice. Landsat-5 image courtesy of the U.S. Geological Survey. We thank the MSc Geosciences students of the University of Münster

enrolled in the course “M35 Erdsystemmodellierung” for their contributions to composite image building, georeferencing, and habitat classification. We are grateful to CycloNet members for discussions.

Funding

Funded by the European Union (ERC, MindTheGap, StG project no 101041077). Views and opinions expressed are however those of the author(s) only and do not necessarily reflect those of the European Union or the European Research Council. Neither the European Union nor the granting authority can be held responsible for them. This study received support from CycloNet project, funded by the Research Foundation Flanders (FWO, grant no. W000522N).

Supplementary materials and code availability

Supplementary data is stored in Zenodo: 10.5281/zenodo.20306840.

Code is available in github: https://github.com/MindTheGap-ERC/TrackingHabitat.git, and zenodo: 10.5281/zenodo.20309343.

Reference:

1. A. Elfeki, F. Dekking, Modelling subsurface heterogeneity by coupled Markov chains: directional dependency, Walther’s law and entropy. *Geotechnical & Geological Engineering* **23**, 721–756 (2005).
2. A. Strasser, "Chapter Three - Cyclostratigraphy of Shallow-Marine Carbonates – Limitations and Opportunities" in *Stratigraphy & Timescales,* M. Montenari, Ed. (Academic Press, 2018), vol. 3, pp. 151–187.
3. G. S. Visher, Use of Vertical Profile in Environmental Reconstruction1. *AAPG Bulletin* **49**, 41–61 (1965).
4. C. E. Brett, Sequence stratigraphy, paleoecology, and evolution; biotic clues and responses to sea-level fluctuations. *PALAIOS* **13**, 241–262 (1998).
5. J. M. Kerr, S. Purkis, B. Riegl, P. Burgess, A quantitative criterion with which to distinguish lithofacies belts from mosaics in carbonate deposystems. *Marine Geology* **436**, 106487 (2021).
6. L. Pomar, Ecological control of sedimentary accommodation: evolution from a carbonate ramp to rimmed shelf, Upper Miocene, Balearic Islands. *Palaeogeography, Palaeoclimatology, Palaeoecology* **175**, 249–272 (2001).
7. L. Tomassetti, L. Petracchini, M. Brandano, F. Trippetta, A. Tomassi, Modeling lateral facies heterogeneity of an upper Oligocene carbonate ramp (Salento, southern Italy). *Marine and Petroleum Geology* **96**, 254–270 (2018).
8. S. R. Jenkins, M. Uyà, Temporal scale of field experiments in benthic ecology. *Marine Ecology Progress Series* **547**, 273–286 (2016).
9. A. Kalman, A. F. Humphreys, Z. Adams, R. Ames, A. R. Marín, A. C. Dempsey, S. J. Purkis, Foraminifera record historical coral-algal phase shifts on Caribbean coral reefs. *Marine Environmental Research* **211**, 107437 (2025).
10. L. R. Hernández-Cruz, S. J. Purkis, B. M. Riegl, Documenting decadal spatial changes in seagrass and Acropora palmata cover by aerial photography analysis in Vieques, Puerto Rico: 1937–2000. *Bulletin of Marine Science* **79**, 401–414 (2006).
11. D. J. Jerolmack, P. Sadler, Transience and persistence in the depositional record of continental margins. *Journal of Geophysical Research: Earth Surface* **112**, (2007).
12. C. E. Brett, A. J. Hendy, A. J. Bartholomew, J. R. Bonelli Jr, P. I. McLaughlin, Response of shallow marine biotas to sea-level fluctuations: a review of faunal replacement and the process of habitat tracking. *Palaios* **22**, 228–244 (2007).
13. J. S. Levinton, *Marine biology: function, biodiversity, ecology* (1995).

14. S. J. Purkis, K. E. Kohler, B. M. Riegl, S. O. Rohmann, The statistics of natural shapes in modern coral reef landscapes. *The Journal of Geology* **115**, 493–508 (2007).
15. S. J. Purkis, A. C. R. Gleason, C. R. Purkis, A. C. Dempsey, P. G. Renaud, M. Faisal, S. Saul, J. M. Kerr, High-resolution habitat and bathymetry maps for 65,000 sq. km of Earth's remotest coral reefs. *Coral Reefs* **38**, 467–488 (2019).
16. P. T. Harris, E. K. Baker, "1 - Why Map Benthic Habitats?" in *Seafloor Geomorphology as Benthic Habitat,* P. T. Harris, E. K. Baker, Eds. (Elsevier, London, 2012), pp. 3–22.
17. T.-L. Loh, S. K. Archer, A. Dunham, Monitoring program design for data-limited marine biogenic habitats: A structured approach. *Ecology and Evolution* **9**, 7346–7359 (2019).
18. C. Lopez-Gamundi, B. B. Barnes, C. Betzler, P. M. Harris, A. M. Oehlert, G. P. Eberli, S. J. Purkis, The sediment budget of Great Bahama Bank—Earth's largest modern carbonate platform. *Geology*, (2025).
19. C. T. Perry, K. M. Morgan, R. T. Yarlett, Reef habitat type and spatial extent as interacting controls on platform-scale carbonate budgets. *Frontiers in Marine Science* **4**, 185 (2017).
20. A. Pohl, M. Laugié, J. Borgomano, J. Michel, C. Lanteaume, C. R. Scotese, C. Frau, E. Poli, Y. Donnadieu, Quantifying the paleogeographic driver of Cretaceous carbonate platform development using paleoecological niche modeling. *Palaeogeography, Palaeoclimatology, Palaeoecology* **514**, 222–232 (2019).
21. P. M. Harris, Holocene marine-cemented sands, Joulters ooid shoal, Bahamas. (1978).
22. E. C. Rankey, S. L. Reeder, "Tidal sands of the Bahamian archipelago" in *Principles of tidal sedimentology* (Springer, 2012), pp. 537–565.
23. S. J. Purkis, P. M. Harris, The Extent and Patterns of Sediment Filling of Accommodation Space On Great Bahama Bank. *Journal of Sedimentary Research* **86**, 294–310 (2016).
24. P. Harris, J. Carlos Laya, M. Frazer, in *Second International Meeting for Applied Geoscience & Energy*. (Society of Exploration Geophysicists and American Association of Petroleum …, 2022), pp. 347–350.
25. K. L. Bergman, H. Westphal, X. Janson, A. Poiriez, G. P. Eberli, "Controlling parameters on facies geometries of the Bahamas, an isolated carbonate platform environment" in *Carbonate depositional systems: assessing dimensions and controlling parameters: the Bahamas, Belize and the Persian/Arabian Gulf* (Springer, 2010), pp. 5–80.
26. S. L. Reeder, E. C. Rankey, Controls on morphology and sedimentology of carbonate tidal deltas, Abacos, Bahamas. *Marine Geology* **267**, 141–155 (2009).
27. A. C. Hine, A. C. Neumann, Shallow Carbonate-Bank-Margin Growth and Structure, Little Bahama Bank, Bahamas1. *AAPG Bulletin* **61**, 376–406 (1977).
28. H. Lantzsch, S. Roth, J. J. G. Reijmer, H. Kinkel, Sea-level related resedimentation processes on the northern slope of Little Bahama Bank (Middle Pleistocene to Holocene). *Sedimentology* **54**, 1307–1322 (2007).
29. T. S. Winkler, P. J. van Hengstum, J. P. Donnelly, E. J. Wallace, R. M. Sullivan, D. MacDonald, N. A. Albury, Revising evidence of hurricane strikes on Abaco Island (The Bahamas) over the last 700 years. *Scientific Reports* **10**, 16556 (2020).
30. M. Wu, P. M. Harris, G. Eberli, S. J. Purkis, Sea-level, storms, and sedimentation–Controls on the architecture of the Andros tidal flats (Great Bahama Bank). *Sedimentary Geology* **420**, 105932 (2021).
31. A. Bruckner, J. Kerr, G. Rowlands, A. Dempsey, S. Purkis, P. Renaud. (Panoramic Press, Great Inagua, Little Inagua and Hogsty Reef, Bahamas, 2014).
32. S. R. Schill, V. P. McNulty, F. J. Pollock, F. Lüthje, J. Li, D. E. Knapp, J. D. Kington, T. McDonald, G. T. Raber, X. Escovar-Fadul, G. P. Asner, Regional High-Resolution Benthic Habitat Data from Planet Dove Imagery for Conservation Decision-Making and Marine Planning. *Remote Sensing* **13**, 4215 (2021).
33. M. Hussain, D. Chen, A. Cheng, H. Wei, D. Stanley, Change detection from remotely sensed images: From pixel-based to object-based approaches. *ISPRS Journal of photogrammetry and remote sensing* **80**, 91–106 (2013).
34. S. Saul, S. Purkis, Semi-automated object-based classification of coral reef habitat using discrete choice models. *Remote Sensing* **7**, 15894–15916 (2015).

35. R. M. Hulshoff, Landscape indices describing a Dutch landscape. *Landscape Ecology* **10**, 101–111 (1995).
36. K. McGarigal, S. A. Cushman, M. C. Neel, E. Ene, FRAGSTATS: spatial pattern analysis program for categorical maps. *Computer software program produced by the authors at the University of Massachusetts, Amherst* **3**, (2002).
37. Y. Zou, T. W. Crowther, G. R. Smith, H. Ma, L. Mo, L. Bialic-Murphy, P. Potapov, K. A. Gawecka, C. Xu, P. J. Negret, T. Lauber, Z. Wu, D. Rebindaine, C. M. Zohner, Fragmentation increased in over half of global forests from 2000 to 2020. *Science* **389**, 1151–1156 (2025).
38. C. N. Drummond, P. J. Dugan, Self-organizing models of shallow-water carbonate accumulation. *Journal of Sedimentary Research* **69**, 939–946 (1999).
39. A. E. Stears, P. B. Adler, S. E. Albeke, D. H. Atkins, J. Studyvin, D. C. Laughlin, plantTracker: An R package to translate maps of plant occurrence into demographic data. *Methods in Ecology and Evolution* **13**, 2129–2137 (2022).
40. P. M. Harris, Facies anatomy and diagenesis of a Bahamian ooid shoal. (1979).
41. J. Meyer, J. Munn, E. Arnaud, J. Kennel, B. Parker, Graphical Shading Logs: An Improved Approach for Collecting High Resolution Sedimentological Data at Contaminated Sites. *Groundwater Monitoring & Remediation* **42**, 59–74 (2022).
42. S. D. Locker, "Origin and depositional history of a semi-enclosed windward lagoon off Great Abaco Island, Bahamas", thesis, University of North Carolina at Chapel Hill (1980).
43. K. M. Mullen, "Lithofacies of the Pliocene-Pleistocene Lucayan Limestone, Great Abaco Island, Little Bahama Bank", thesis, Old Dominion University (1993).
44. P. Burgess. (https://github.com/MindTheGap-ERC/Stacker, 2019).
45. E. C. Geyman, A. C. Maloof, B. Dyer, How is sea level change encoded in carbonate stratigraphy? *Earth and Planetary Science Letters* **560**, 116790 (2021).
46. J. Hidding, E. Jarochowska, N. Hohmann, X. Liu, P. Burgess, H. Spreeuw, CarboKitten. jl–an open source toolkit for carbonate stratigraphic modeling. *EGUsphere*, (2025).
47. S. Vitousek, K. Vos, K. D. Splinter, L. Erikson, P. L. Barnard, A Model Integrating Satellite-Derived Shoreline Observations for Predicting Fine-Scale Shoreline Response to Waves and Sea-Level Rise Across Large Coastal Regions. *Journal of Geophysical Research: Earth Surface* **128**, e2022JF006936 (2023).
48. C. Boström, E. L. Jackson, C. A. Simenstad, Seagrass landscapes and their effects on associated fauna: a review. *Estuarine, Coastal and shelf science* **68**, 383–403 (2006).
49. W. Schlager, "Sedimentation rates and growth potential of tropical, cool-water and mud-mound carbonate systems" in *Carbonate Platform Systems: Components and Interactions,* E. Insalaco, P. W. Skelton, T. J. Palmer, Eds. (Geological Society of London, 2000), vol. 178, pp. 0.
50. L. Telesca, A. Belluscio, A. Criscoli, G. Ardizzone, E. T. Apostolaki, S. Fraschetti, M. Gristina, L. Knittweis, C. S. Martin, G. Pergent, A. Alagna, F. Badalamenti, G. Garofalo, V. Gerakaris, M. Louise Pace, C. Pergent-Martini, M. Salomidi, Seagrass meadows (Posidonia oceanica) distribution and trajectories of change. *Scientific Reports* **5**, 12505 (2015).
51. M. v. Keulen, M. A. Borowitzka, Seasonal variability in sediment distribution along an exposure gradient in a seagrass meadow in Shoalwater Bay, Western Australia. *Estuarine, Coastal and Shelf Science* **57**, 587–592 (2003).
52. E. C. Rankey, On the Interpretation of Shallow Shelf Carbonate Facies and Habitats: How Much Does Water Depth Matter? *Journal of Sedimentary Research* **74**, 2–6 (2004).
53. C. M. Bertelli, H. J. Stokes, J. C. Bull, R. K. F. Unsworth, The use of habitat suitability modelling for seagrass: A review. *Frontiers in Marine Science* **Volume 9 - 2022**, (2022).
54. D. M. Anderson, Attenuation of millennial-scale events by bioturbation in marine sediments. *Paleoceanography* **16**, 352–357 (2001).
55. T. J. Kooistra, A. M. de Boer, T. J. Bouma, N. Pannozzo, S. G. Pearson, A. van der Spek, H. de Stigter, J. Wallinga, R. Witbaard, K. Soetaert, Worms or storms? Distinguishing bioturbation from physical mixing using multiple tracers. *EGUsphere* **2025**, 1–39 (2025).
56. H. S. Greig, P. A. McHugh, R. M. Thompson, H. J. Warburton, A. R. McIntosh, Habitat size influences community stability. *Ecology* **103**, e03545 (2022).

57. N. G. Pisias, Geologic time series from deep-sea sediments: Time scales and distortion by bioturbation. *Marine Geology* **51**, 99–113 (1983).
58. J. E. Jelbart, P. M. Ross, R. M. Connolly, Edge effects and patch size in seagrass landscapes: an experimental test using fish. *Marine Ecology Progress Series* **319**, 93–102 (2006).
59. P. M. Burgess, CarboCAT: A cellular automata model of heterogeneous carbonate strata. *Computers & geosciences* **53**, 129–140 (2013).
60. P. M. Burgess, D. A. Pollitt, The origins of shallow-water carbonate lithofacies thickness distributions: one-dimensional forward modelling of relative sea-level and production rate control. *Sedimentology* **59**, 57–80 (2012).
61. P. M. Burgess, The nature of shallow-water carbonate lithofacies thickness distributions. *Geology* **36**, 235–238 (2008).
62. R. Schumer, D. J. Jerolmack, Real and apparent changes in sediment deposition rates through time. *Journal of Geophysical Research: Earth Surface* **114**, (2009).
63. N. Hohmann, J. R. Koelewijn, P. Burgess, E. Jarochowska, Identification of the mode of evolution in incomplete carbonate successions. *BMC Ecology and Evolution* **24**, 113 (2024).
64. S. Davies Neil, P. Veenma Yorick, A. Craig James, A. Allport Hamilton, J. McMahon William, P. Shillito Anthony, Time, space and synoptic topography: how to read outcrops as a granular record of Earth history. *Geological Society, London, Special Publications* **556**, 15–71 (2025).
65. M. Tucker, Shallow-marine carbonate facies and facies models. *Geological Society, London, Special Publications* **18**, 147–169 (1985).
66. S. O. Egenhoff, A. Peterhänsel, T. Bechstädt, R. Zühlke, J. Grötsch, Facies architecture of an isolated carbonate platform: tracing the cycles of the Latemar (Middle Triassic, northern Italy). *Sedimentology* **46**, 893–912 (1999).
67. D. De Vleeschouwer, L. M. Percival, N. M. Wichern, S. J. Batenburg, Pre-Cenozoic cyclostratigraphy and palaeoclimate responses to astronomical forcing. *Nature Reviews Earth & Environment* **5**, 59–74 (2024).
68. M. Wang, M. Li, E. A. Hajek, D. B. Kemp, Y. Wu, H. Zhu, C. Huang, H. Zhang, K. Ji, R. Zhang, Assessing the preservation of orbital signals across different sedimentary environments: Insights from stochastic sedimentation modeling. *Earth and Planetary Science Letters* **642**, 118866 (2024).

Supplementary materials

For

Stratigraphy as a low-pass filter: selective preservation of spatial variability on a Holocene carbonate platform

Xianyi Liu *et al*.

*Email address: x.liu6@uu.nl;

This PDF file includes:

Supplementary text

Figures S1 to S12.

Tables S1 to S7.

Equations S1 to S5.

Other Supplementary Materials for this manuscript include the following:

Data S1: original individual vintage image.

Data S2: assembled vintage image.

Data S3: ArcGIS files with segmented vintage/modern images.

Data S4: Interpreted habitat maps (shapefile).

Data S5: Spreadsheet containing area and perimeter statistics for individual patches.

Data S6: Spreadsheet containing tracking results.

Data S7: Input and output of STACKER.

Supplementary Text

Materials for interpretation

The assembled photo

The assembled photos from the Joulters Cays and the North Abacos, are stored at Data S3.

Historical satellite imagery

To study the inter-decadal facies changes, we applied the same facies classification to historical images: 1) 1984 by Landsat 5 (Landsat 5 image courtesy of the U.S. Geological Survey); 2) a set of two groups of satellite images taken before and after 2016 hurricane Matthew (Copernicus Sentinel data [2016]). The resolution of the 1984 image was ~30 m. This timeslice may not allow resolving small objects (e.g., patch reefs), but it might be useful for increasing confidence level of interpretations of large objects (e.g., barren sand, seagrass meadows, etc.). For the 2016 satellite images, we chose satellite images before and after hurricane Matthew (August 2016 and December 2016, respectively), specifically looking at whether the distribution of active ooid sandbars and seagrasses had changed or not. The images are obtained by the European Space Agency Sentinel 2 satellite with horizontal resolution of 10×10 m. Hurricane Matthew (October 5, 2016) was chosen because it passed through the Bahamas with category 5 strength and may have had sufficient power to change the habitat distribution.

Modern digital elevation model of the Bahamas

We obtained the DEM (digital elevation model) of both the Joulters Cays and North Abacos with a resolution of 10 m (from Tcarta, the link: https://caribgeoportal.maps.arcgis.com/, name: Bathymetry of Bahamas Lucayan Archipelago). This DEM data is derived from Sentinel-2 satellite images. This DEM has a resolution 10 times coarser than the resolution of aerial and modern satellite images we used and therefore could only be used for rough comparison to the vintage image (~1 m resolution).

Applying object-based classification

The assembled photos are fed into eCognition® for object-based classification.

Segmentation

The input assembled photos are segmented into different fields by applying multi-resolution segmentation algorithm. This is a bottom-up segmentation process that consecutively merges pixels or existing image objects. The basic parameters used in this method are listed in the following table S1.

Table S4.Parameters for segmentation.

Parameter	Value
Scale	60
Shape	0.9
Compactness	0.6

Object-based classification

After the photo was segmented, we can choose the examples ready for object-based classification training according to Figure 2 in the maintext. In this context, we chose SVM (support vector machine) algorithm to classify the segmented photos. This is because after trying all the embedded

algorithm, the SVM algorithm presents the highest accuracy and requires least time to process in this context. The parameters needed are presented below:

Table S5. Parameters for object-based classification

Features	Mean, Brightness, Shape, Roundness, Max Differences
Kernel type	Linear
C	2

Historic satellite images (1984)

The image is downloaded from USGS EarthExplorer. The resolution of this image is lower than the vintage photo and the modern satellite images, and therefore, we cannot use this information to compare with the 1945 or 2019 data, but instead we use this material as an intermediate check for interpretation. The results suggest that the habitats are distributed as belt-like shape, and they distributed from shallow to deep as: microfilm-cemented-sand/island to active ooid sand, to seagrass meadow/macroalgae-cemented-sand and to hardground. Such distributions are similar to the results from both 1945 and 2019 results (Figure 3, 5 in the main text). The 1984 interpretation suggests confirms the approximate spatial distribution of the habitats, and confirmed the validity of the interpretation. The comparison between the 1984 annotated image and the vintage image is described in Figure S1.

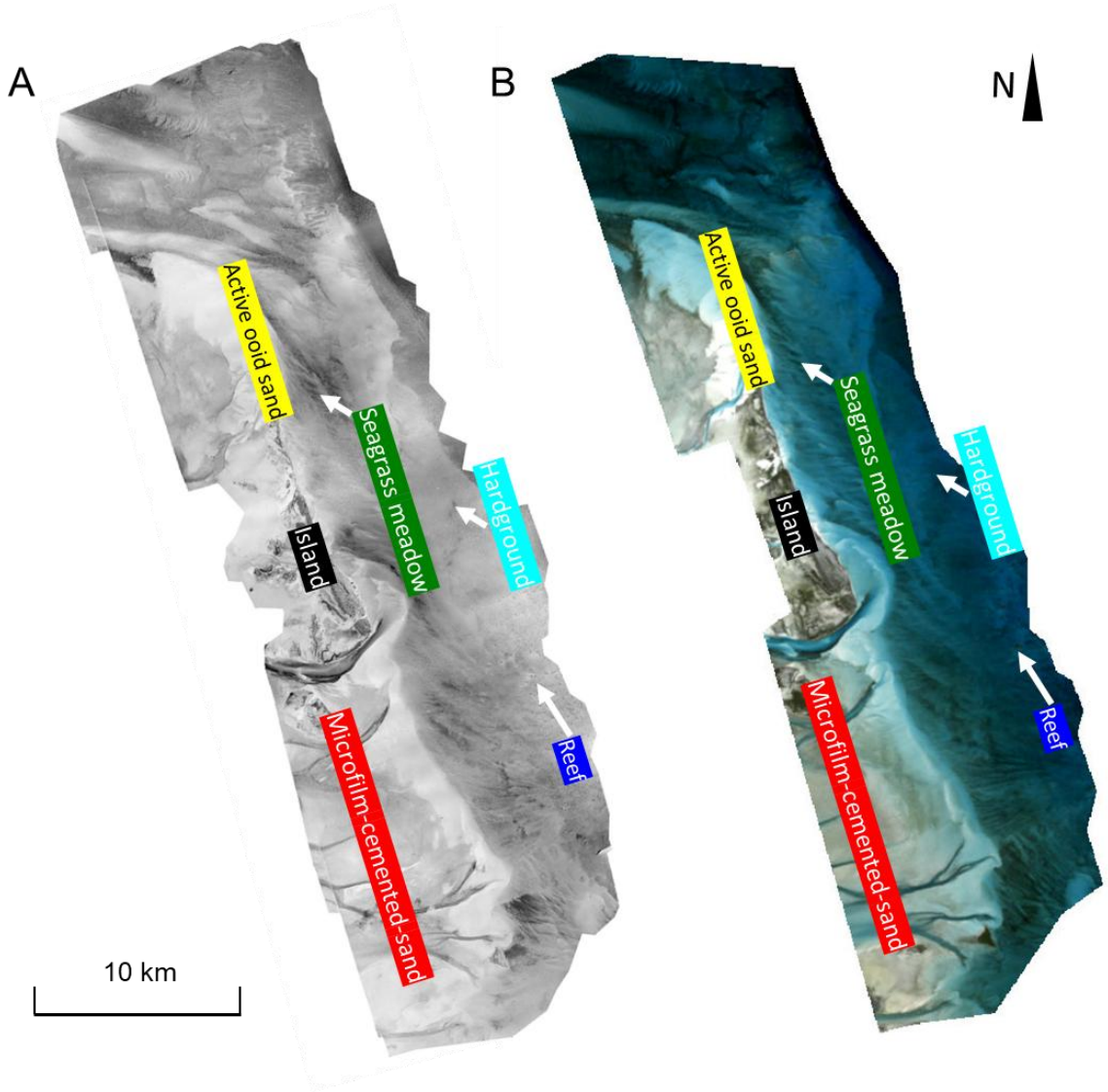

Figure S3. A: annotated assembled vintage photo in the Joulters Cays. B: annotated satellite image (1984) in the Joulters Cays. The approximate spatial distribution of habitats agrees.

Historical satellite image (2016, pre- and post- hurricane)

Before analyzing the change patterns and rates at the decadal scale, we first need to exclude the possibility that the observed changes are short-term (i.e., seasonal, changes after extreme events, etc.). Tropical hurricanes are regarded as one of the important short-term causes for changes in tropical geomorphology and habitat distribution (*1, 2*).

Pre- and post-hurricane satellite images (the image is downloaded from Copernicus) from Joulters Cays (Figure S2) indicate that changes in habitat distribution due to hurricane Matthews (2016) were negligible (**Error! Reference source not found.**S2). This was true also for Hurricane Andrews (1992): the external boundaries of sand shoals were relatively unchanged after hurricane events and the internal sand shoal changes may not be preserved in long-term (*3, 4*). Certain crests of sand bars in seagrass meadows showed signs of being re-activated (i.e., bright whitish bands, indicated in Figure S2 E, F, red arrow), but overall the distribution of seagrass meadows remained unchanged. These limited observations support the hypothesis that hurricanes have limited effects on habitat distribution (*5, 6*). However, the hypothesis remains to be tested with a larger number of hurricane events. We cannot exclude an amalgamated influence of recurring hurricanes. In addition, Major (*4*) suggested

that a very thin layer of poorly-sorted sand might be transported seaward after hurricanes and may not be resolved in these satellite images at 10 m resolution.

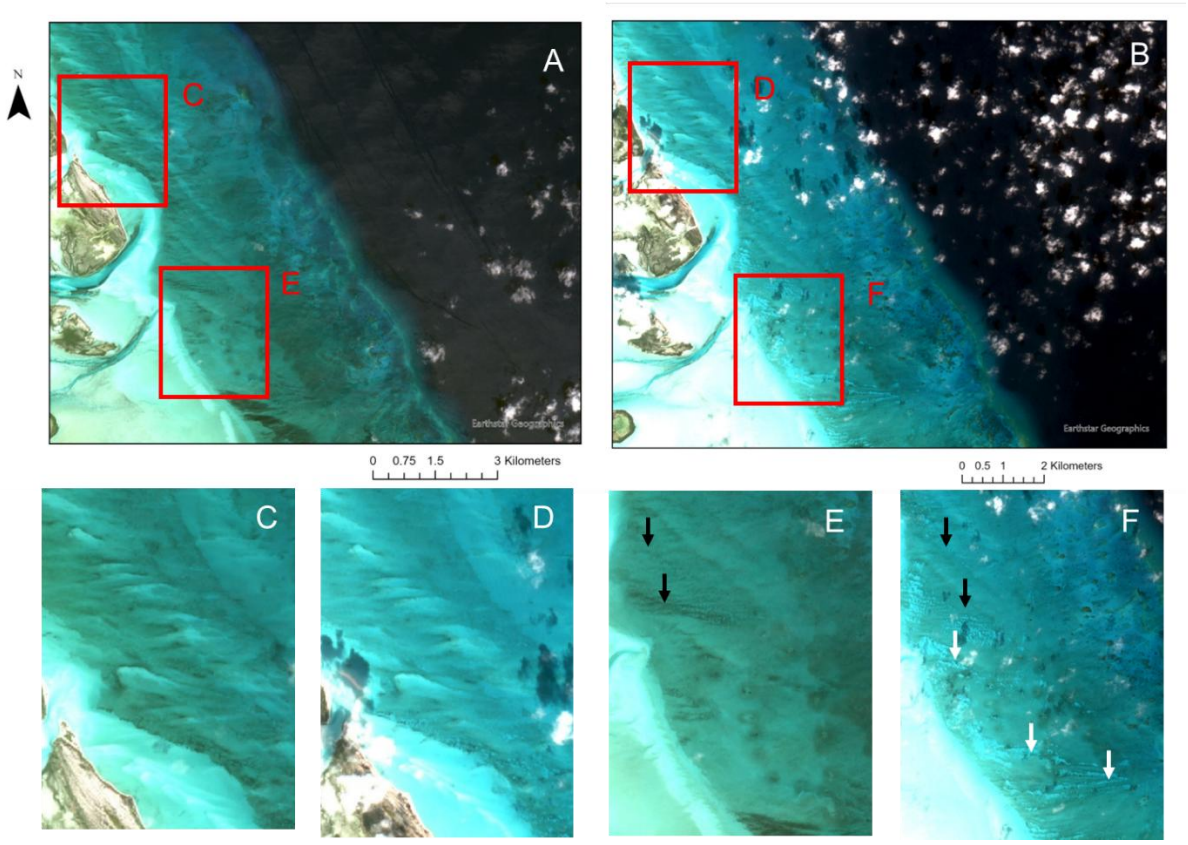

Figure S4. Pre- and post-hurricane satellite images from Joulters Cays (Copernicus Sentinel data [2016]). A: pre-hurricane (6-Sep-2016) and B: post-hurricane (14-Dec-2016). C, D, E, F are zoomed-in panels to show the details of seagrass-sand boundaries. Black arrows: re-activated sand bar crests after hurricane. White arrows: seagrass distribution.

Spatial heterogeneities calculation

The original data for spatial heterogeneity calculation were presented in Data S6. This includes edge length and area for each patch from both the North Abacos and the Joulters Cays region.

Explanation of the metrics:

1. Largest Patch Index (LPI). This metric indicates the proportion of the largest patch in the total area of the same habitat, and is classified as a metric to measure dominance in some studies (*7*). This metric measures the connectivity of habitats: lower LPI indicates the habitats in the study area are more fragmented (low connectivity) and have higher spatial heterogeneities (*8*).

$$LPI = \frac{Max(Patch\ Area)}{\sum Area\ of\ individual\ patch} \times 100\% \quad \text{(Eqn. S1)}$$

2. Number of Patches (NP). This structure-focused metric measures how many distinctive patches could be identified in the observing area. In general, high NP means the habitats are divided into fragmented pieces and have higher spatial heterogeneities (*8*).
3. Mean patch area (MPA). This is a structure-focused metric and smaller MPA may indicate the habitats are more fragmented and heterogeneous (*8*).

$$MPA = \frac{\sum Area\ of\ individual\ patch}{Number\ of\ patches} \times 100\,\% \quad \text{(Eqn. S2)}$$

4. Edge Density (ED). This is a structure-focused metric. This metric measures the edge effects of the patches. The edge effect is crucial for the shrinking and expansion of patches. This is because the ambient physical environment and biological interactions outside and inside of an edge are different (*9*). Higher ED means these habitat patches are subject to higher influence from outside of the patch edges. We also apply the edge density metric to individual patches (Eqn S4).

$$ED = \frac{\sum Edge\ of\ individual\ patch}{\sum Area\ of\ individual\ patch} \times 100\% \quad \text{(Eqn. S3)}$$

$$ED\_i = \frac{Edge\ of\ individual\ patch}{Area\ of\ individual\ patch} \times 100\% \quad \text{(Eqn. S4)}$$

5. Spatial entropy (SE) is a proxy based on cellular data. It is defined in equation 5 (*10*):

$$SE = \frac{Number\ of\ disimilar\ connections}{Number\ of\ total\ connections} \quad \text{(Eqn. S5)}$$

Habitat tracking

The tracking method is described and illustrated in the main text. Herein, we present further details of the process.

The packages we used in the workflow are described below (Table S3):

Table S6. Packages used in the workflow.

Package name	Language
PlantTracker	R
ArchGDAL	Julia
Statistics	Julia
GeoMakie	Julia

PlantTracker

The parameters used in *PlantTracker* is listed below (Table S4). For the definition of them please refer to the original paper (*11*).

Table S7. Parameters used in PlantTracker.

Parameter	Value
dorm	80
buff	20
buffGenet	50
clonal	TRUE
aggByGenet	TRUE

Tracking visualization

The tracking results were visualized by GeoMakie and are presented in the following figure S3-S7.

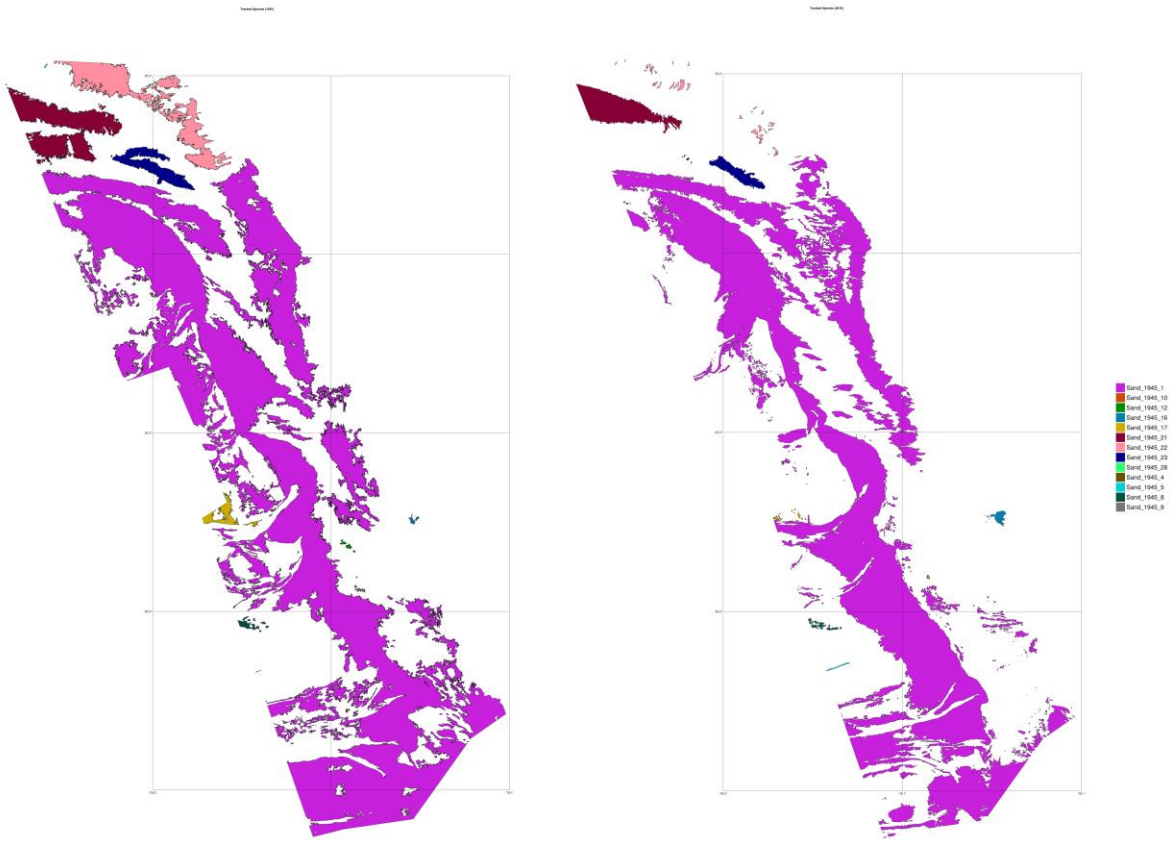

Figure S5. Tracking result for habitat ‘active ooid sand’. Left: 1945; Right: 2019. Same color indicates the patch shares the same track ID (i.e., they are the same patch in this context).

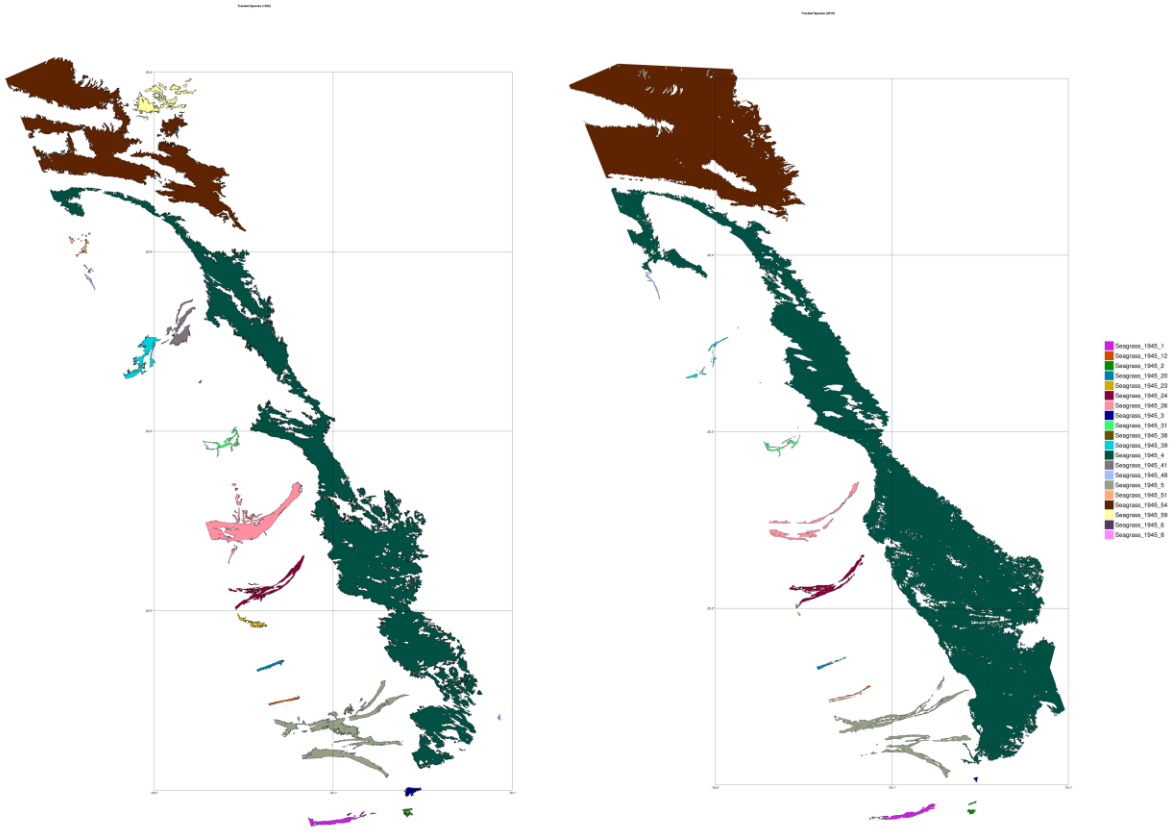

Figure S6. Tracking result for habitat ‘Seagrass meadow’. Left: 1945; Right: 2019. Same color indicates the patch shares the same track ID (i.e., they are the same patch in this context).

Figure S7. Tracking result for habitat ‘Reef’. Left: 1945; Right: 2019. Same color indicates the patch shares the same track ID (i.e., they are the same patch in this context).

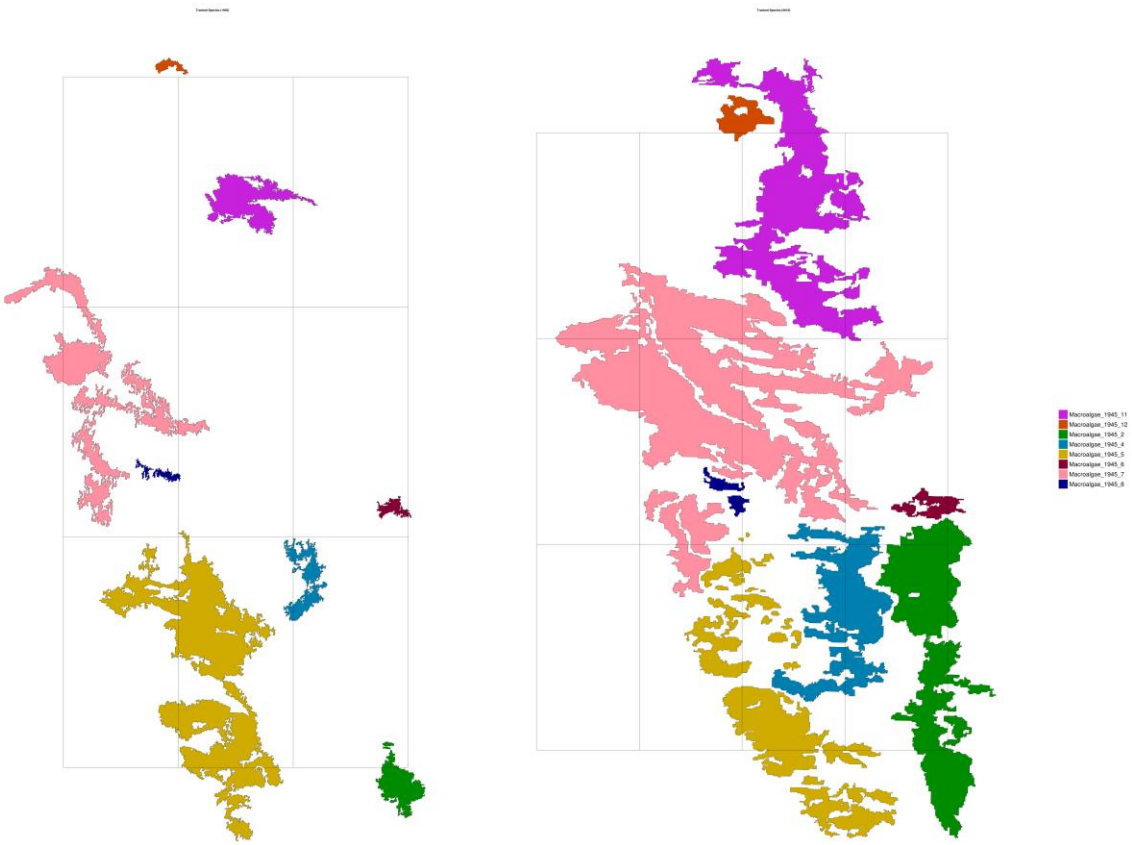

930

931 Figure S8. Tracking result for habitat ‘Macroalgae-cemented-sand’. Left: 1945; Right: 2019. Same
932 color indicates the patch shares the same track ID (i.e., they are the same patch in this context).

933

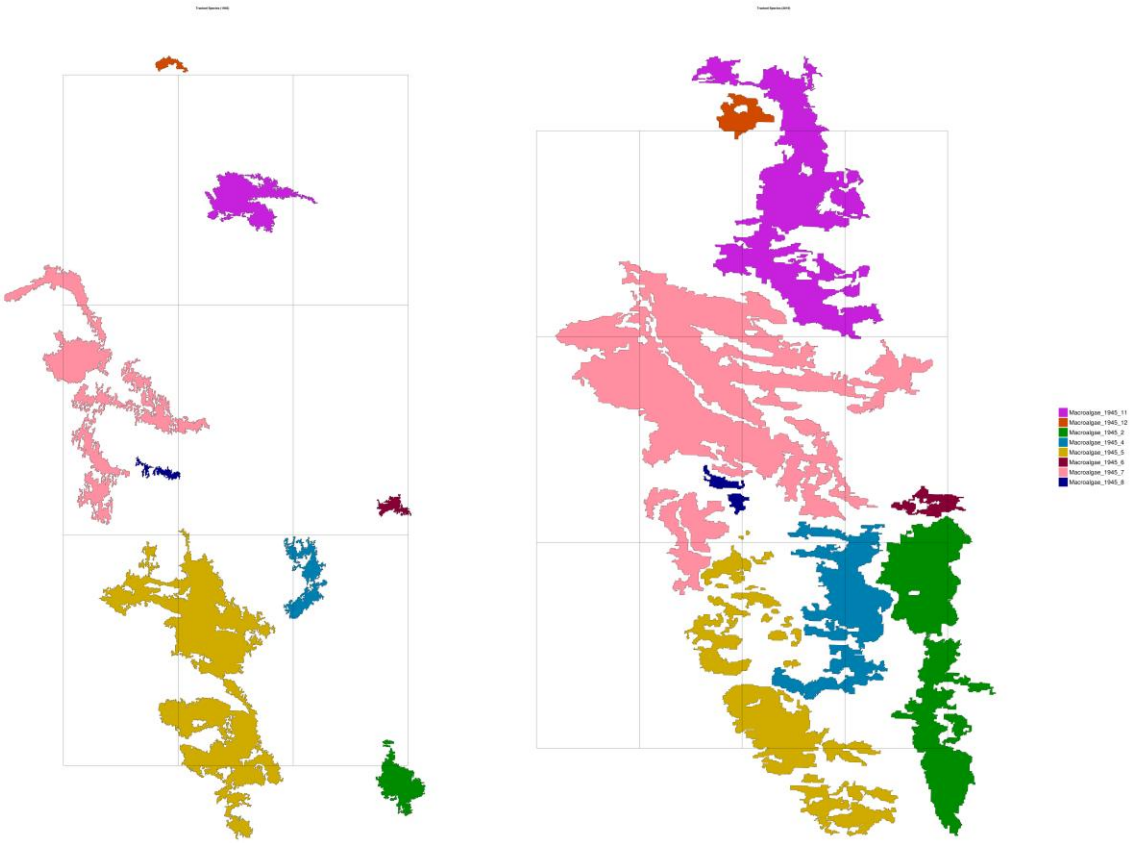

Figure S9. Tracking results for habitat ‘Microfilm-cemented-sand’. Left: 1945; Right: 2019. Same color indicates the patch shares the same track ID (i.e., they are the same patch in this context).

The migration rates and direction are summarized in excel sheet stored in Data- S6. They are also visualized as rose map in the Figure S6.

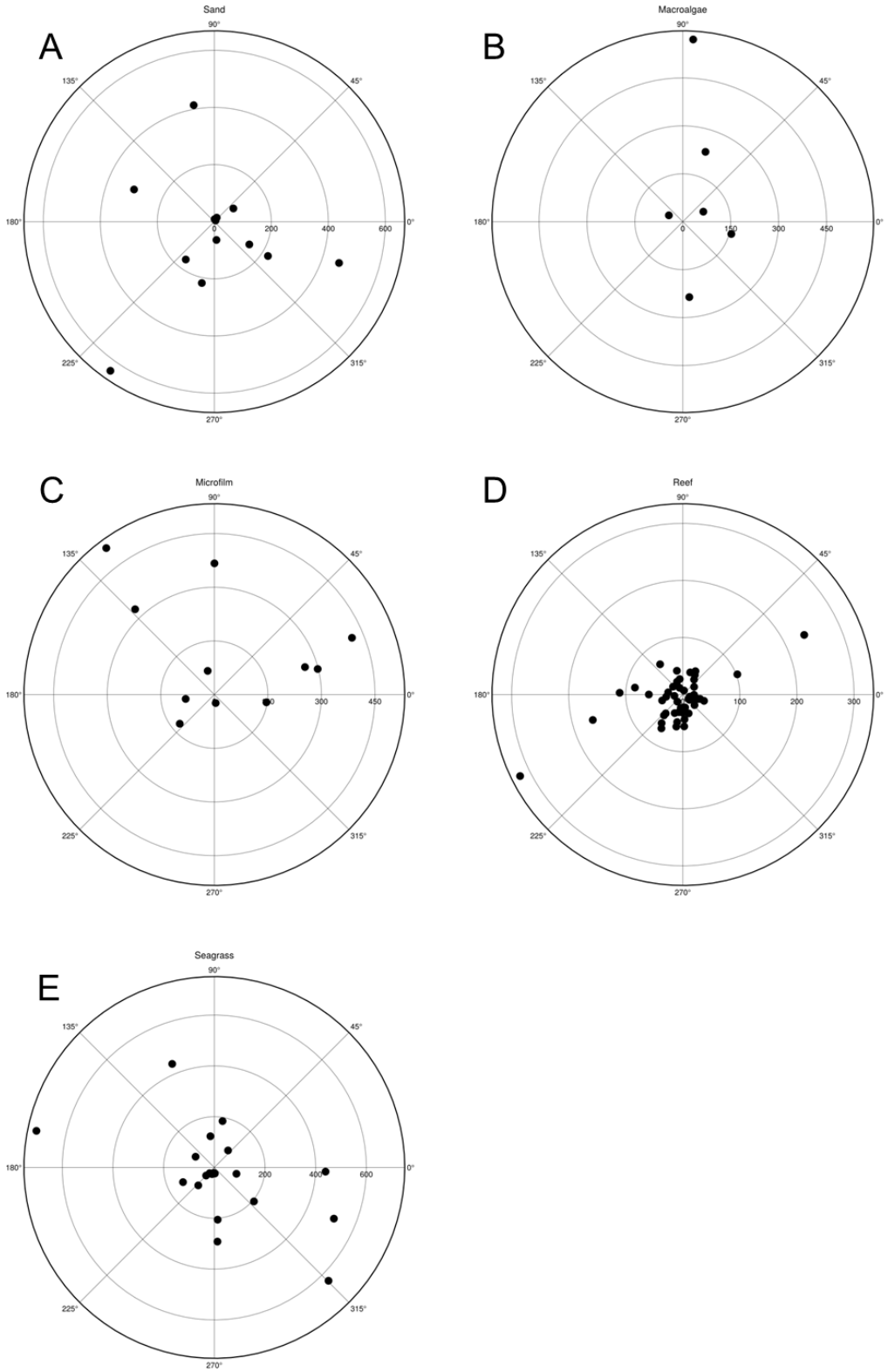

940

941 Figure S10. Visualization of migration rates and direction for each habitat. A: active ooid sand; B:
942 Macroalgae-cemented-sand; C: Microfilm-cemented-sand; D: Reef; E: Seagrass meadow. The radius
943 indicates the migration rates of each patch in units of meters in the observational timespan, while the
944 degrees on the circle indicate the migration directions of each patch.

Patch size and persistence time

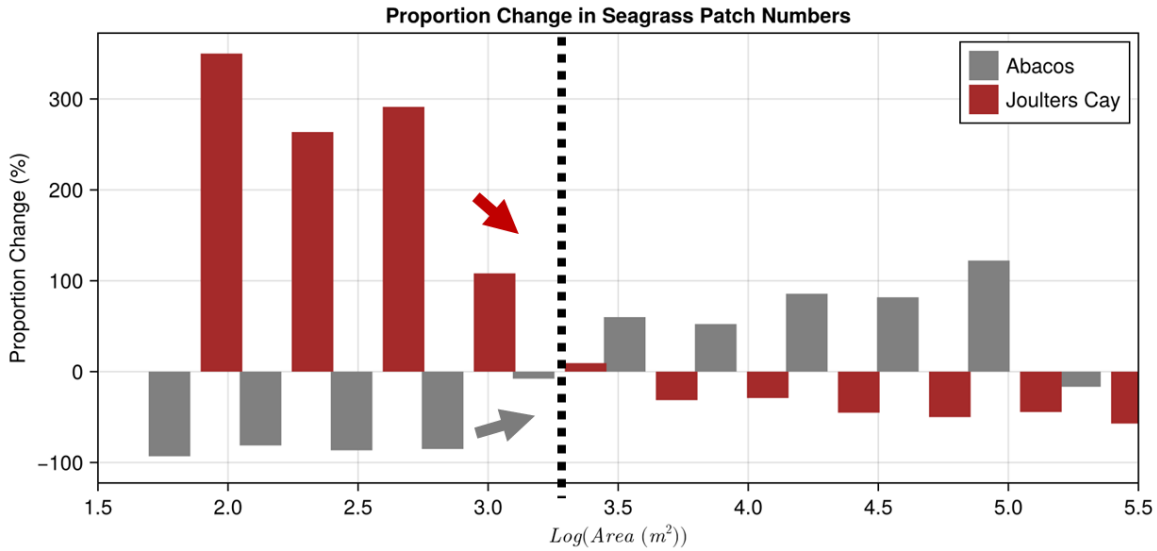

Figure S11. Proportional changes of the number of patches from 1945 to 2019 per area bin.

STACKER

The introduction of STACKER has been described in the main text, and the model is stored on github platform (git@github.com:MindTheGap-ERC/Stacker.git). The copy of this model used in this study is stored in the github repository: https://github.com/MindTheGap-ERC/TrackingHabitat.git. A manual can be found at https://mindthegap-erc.github.io/Stacker/. The input files for STACKER are stored separately in Data S8. Key inputs and assumptions are presented in the following table S5:

Table S8. Default parameters used as STACKER input. These parameters were used for the null scenario (S0),

Parameter	Value
Number of grids of on-shore off-shore direction	100
Number of grids of along-shore direction	100
Grid length of on-shore off-shore direction	0.25 km
Grid length of along-shore direction	0.05 km
Model duration	8 kyr
Timestep	80 yr
Subsidence rate	20 m/Myr
Tidal range	1 m
Number of facies	5
Number of facies mosaic elements	25 (i.e., 5 patch aggregates for each facies)
Migration mode for facies elements	biased random walk
Boundary condition	Reflected

Facies selection	Based on production

Obtaining production rate for each facies

The production rate used in table S6 is obtained from one of the most recent published compilations (*5*). This work reported the production rate with units of g (calcite) × m^{-2} yr^{-1} and we convert the values to m/Myr used in the model. Unit conversion assumed the density of calcite = 2700 kg/m^3, and porosity of 0.25. The conversion is based on the following equation (Equation S6).

$$P\left(unit\ by \frac{m}{Myr}\right) = \frac{P(unit\ by\ g \times\ \mathrm{m}^{-2}\ \mathrm{yr}^{-1})}{\left(density\ (unit\ by \times\ kg\ \mathrm{m}^{-3}) \times (1 - porosity)\right)} \times 1000 \quad \text{(Eqn. S6)}$$

The median and the highest production rates from the published compilation (*5*) are listed in the following table S6 in 'reported median production rate' and 'reported highest production rate'. Accordingly, the converted production rates based on equation S6 are listed in 'converted median production rate' and 'converted highest production rate'.

Table S9. Production rates used in this study, obtained from values published by Lopez-Gamundi et al. (*5*). Note that the original reported median production rate for active ooid sand is 165 g (calcite) × m^{-2} yr^{-1}, however, their calculations accidentally multiplied by 0.5 twice and thus we restored the value to 330 g (calcite)/m^2 yr herein.

Facies	Reported median production rate	Converted median production rate	Reported highest production rate	Converted highest production rate
Unit	g (calcite) × m^{-2} yr^{-1}	m/Myr	g (calcite) × m^{-2} yr^{-1}	m/Myr
Active ooid sand production rate	330	160	3000	1500
Reef production rate	1120	600	2200	1200
Seagrass meadow production rate	410	200	840	400
Macroalgae-cemented-sand production rate	405	190	850	380
Microfilm-cemented-sand production rate	85	40	180	90

The results of the STACKER

The virtual core results of the STACKER are shown in the main text. The cross-section results are displayed in the following Figure S10.

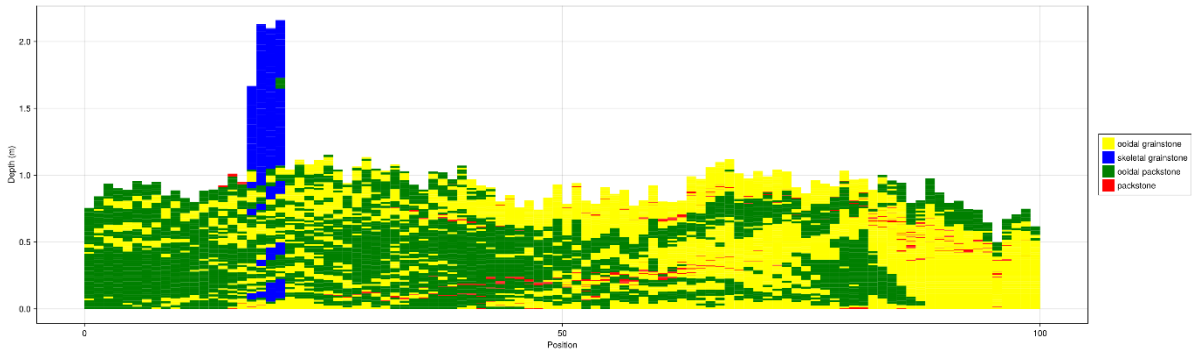

Figure S10. Along-shore cross section of sediment profile for the null scenario S0.

Modeling assumptions and sensitivity of the results to these assumptions

Walther's law does not specify the exact process to translate 2D spatial data into 1D stratigraphic data. Herein, STACKER creates stratigraphy by migrating the habitat patches following the distribution obtained from empirical observations between 1945 and 2019. To achieve this, we make assumptions on:

1. The resolution at which stratigraphic data is recorded,
2. Sediment production rates,
3. Migration algorithm,
4. Dynamics of patches,
5. Patch statistics (including number, dimensions, and geometry) being stationary.

We carried out sensitivity tests addressing the impact of the first four assumptions, corresponding to sensitivity testsS1 to S4.

Scenarios S1: Observational resolution

S1a and S1b have the same default settings as S0, but the virtual cores are then smoothed with a 5 and 10 cm window respectively (Figure7 E, F in the main text).

Scenario S2: Sediment production

Given that each patch has its own dynamic parameters and migration pathways, the patches can overlap with each other. In this case, the facies (or habitat type) to be recorded are set to be the facies with a higher production rate. The S2 scenario used the highest production rates of reported values from previous work (*5*). In this case, the sequence of facies selection when they overlap becomes: active ooid sand > reef > seagrass meadow > macroalgae-cemented-sand > microfilm-cemented-sand, instead of the default sequence of: reef > seagrass meadow > macroalgae-cemented-sand > active ooid sand > microfilm-cemented-sand. By doing so, we tested how facies selection influences the modelling results.

Scenario S3: migration algorithm

We used biased random walk to extrapolate the migration of patches, because the migration of each patch does not take place uniformly in the same direction. This approach had been employed in previous work (*12*). We further tested the scenario of using the 'steepest gradient' algorithm instead of random walk, also following other studies (scenario S3 in Table S6) (*12*).

Scenario S4: Dynamics of patches

It is impossible to know the exact migration route and rate for each habitat patch over the duration of the modelling. Therefore, we have to assume that the observation timespan can be extrapolated for the modelling timespan (8 kyr). To explore how the results would change if the observed dynamics were

not representative for the 8 kyr, we conducted a sensitivity test assuming migration rates equal to 1/10 of those in the null scenario (scenario S4 in Table S6).

Table S10. Sensitivity tests of STACKER parameters.

Scenario	Major changes
S1a	Data smoothed with 5 cm window
S1b	Data smoothed with 10 cm window
S2	Change production rate to the high end of reported range
S3	Migration dynamics changed from 'Randomwalk' to 'Steepest gradient'
S4	10 times decrease in migration rates for each patch

Influence of the exclusion of small patches

Not all patches were tracked by *PlantTracker* and, therefore, not all patches observed in spatial data were fed into STACKER model. This raises concerns over artificially decreasing spatial heterogeneities when converting observed data into model input. Herein, we test this concern by calculating the spatial entropy (SE) of the gridded original interpreted habitat maps (with varying grid size) and comparing it with the input map of STACKER (Figure S11).

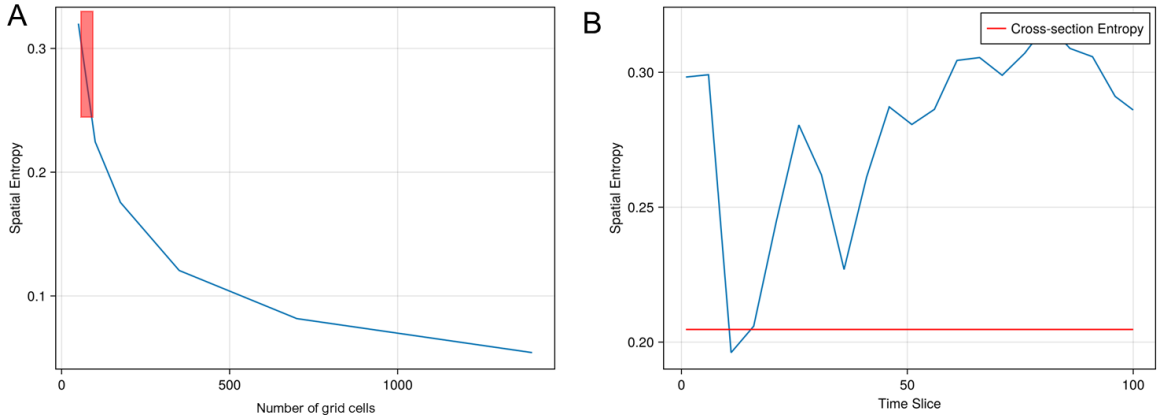

Figure S11. A: Spatial entropy changes with grid size (iso-heterogeneity curve). The thin red box at the left indicates the SE and grid size of STACKER input data. B: Spatial entropy of the horizontal map for each timestep in STACKER.

As grid size increases (the number of grid cells decreases), spatial entropy increases. However, this does not mean the downscaled maps became more heterogeneous, as SE values could not be compared directly with different grid sizes. Rather, it is a scale-dependent benchmark line for SE

proxy. This benchmark line suggests that if the habitat map is downsampled to 100 × 100, the SE value should be around 0.3. We calculated the SE of the STACKER maps at each timeslice and the SE was at quasi-steady-state between the range of 0.25 and 0.35, comparable to that of the downsampled habitat map (Figure S11). This test suggests the incomplete input of patches has minimum influence on the reduction of spatial heterogeneities in model. This result agrees with previous studies suggesting that a loss of some spatial resolution is acceptable (13).

1035

1036

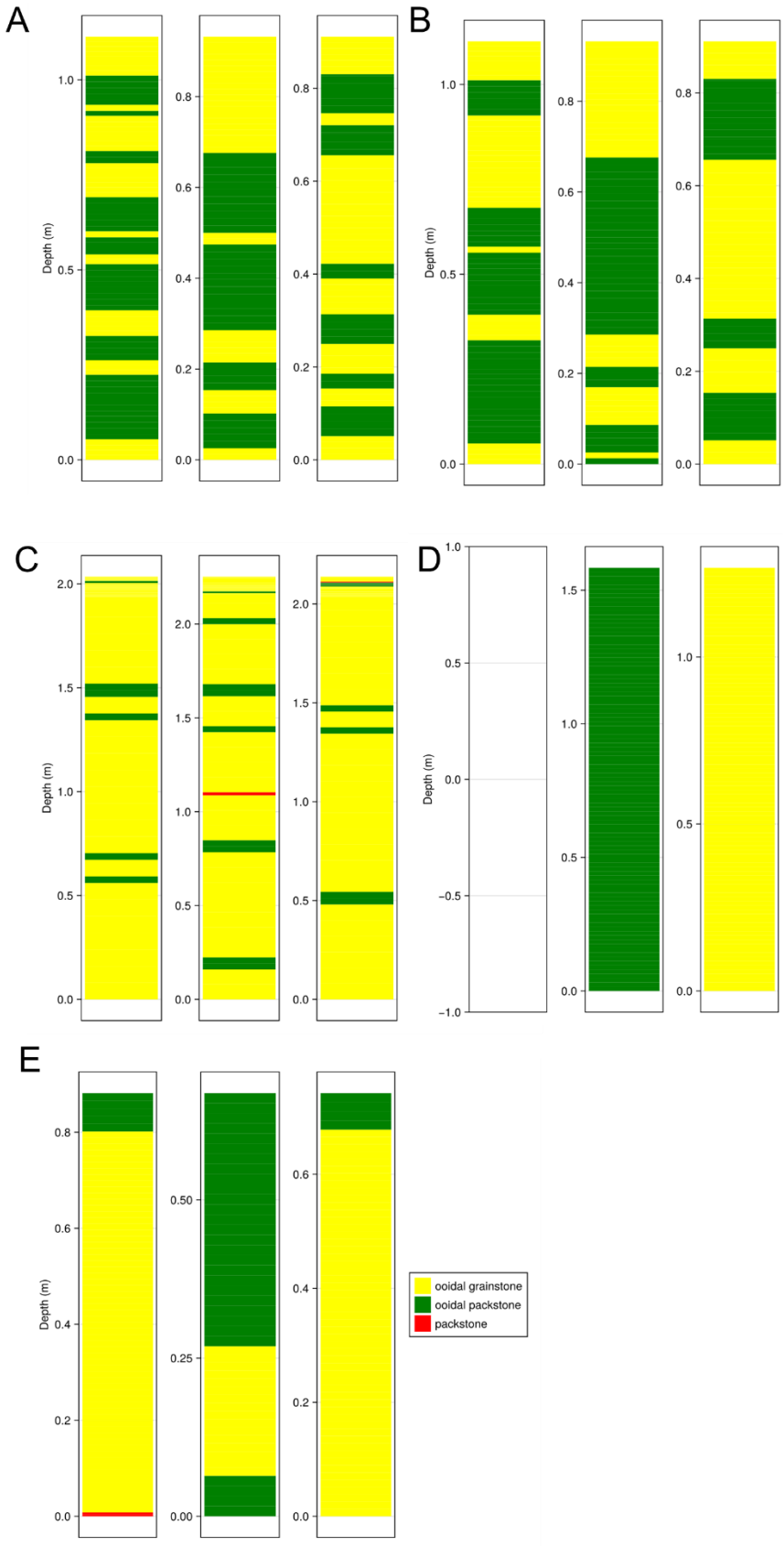

1037

Figure S12. The results of STACKER sensitivity tests listed in table S6. A: Virtual cores for S2.S1a. B: Virtual cores for S31b. C: Virtual cores for S2. D: Virtual cores for S3. E: Virtual cores for S4.

The results of S2 (Figure S12C) indicate that higher production rate and changes in facies selection would lead to the active ooid sand dominating in the virtual cores, in contrast to the sedimentary cores, where ooid packstone and packstone are similarly abundant. Meanwhile, this scenario still results in more frequent facies alternation than in the sedimentary cores. The results of S3 (Figure S12D) are unrealistic: The sedimentation is thoroughly uneven spatially and a part of the modeling box receives a limited amount of sediment (~0.0 m as shown in the leftmost core of S10D, compared to > 1 m as shown in Figure 10 of the main text), contradicting what we observed in empirical cores. The box areas that receive a sufficient amount of sediment also show more frequent facies alternations than the sedimentary cores. The results of S4 (Figure S12 A) show thick facies units and the frequency of facies alternations are similar to those in the sedimentary cores, although the modelled thickness of virtual cores (~0.5 m) is lower than in the sedimentary cores (~1 to 5 m), and the modelled cross-section showed extremely uneven distribution of sediments (Data S7). This result implies that the observations of patch dynamics over multi-decadal timescales are not representative of geological timescales.

Water depth and seagrass meadow distribution map

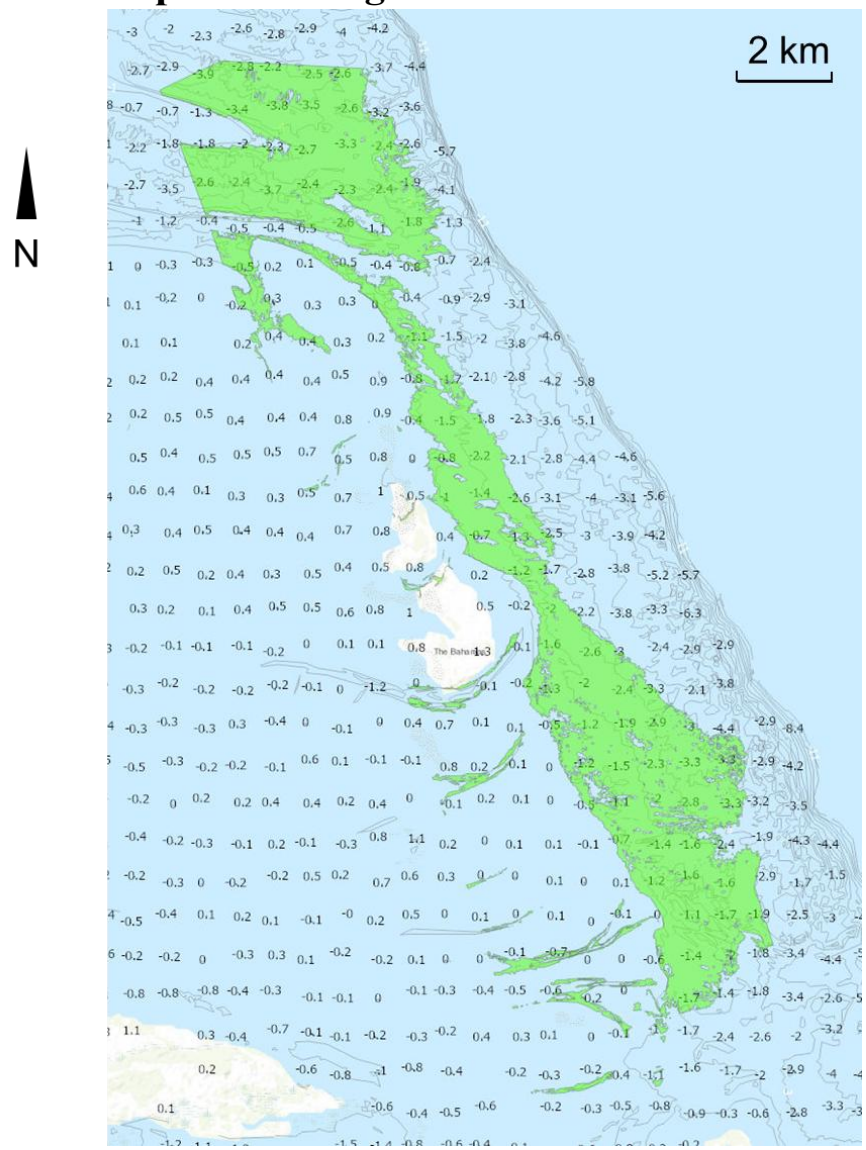

Figure S13. Relationship between water depth and seagrass meadow distribution. The basemap of this figure comes from TCarta DEM (https://caribgeoportal.maps.arcgis.com/

The seagrass meadows are mainly distributed in the water depth of ~1 to 3 m (Figure S13). However, their distribution also relies on the availability of soft bottom, which is mostly located in the western part of the region. In hardground-dominated areas, seagrass meadows are absent.

Source to sink calculation

The growth of islands at both Joulters Cays and North Abacos mainly takes place on the lee side of the island (**Error! Reference source not found.**3,5). This is because the wave energy has been d issipated in these regions, thus making them suitable for sand deposition. In this study we observe net growth of islands (i.e., expansion), rather than lateral migration. The rates of shoreline shift of islands at Joulters Cays (mean = 1.9 m/y) are high compared to the atolls in the Indian Ocean (<0.27 m/y) (*14*). Considering the main sediment in this region is ooidal sand, which has relatively short net transport length (*6*), we assume that ooid sand shoals can be treated as a local source of sediment, and islands as a local sediment sink. In our simple source-to-sink calculation, the 'source' will be

calculated as carbonate production in the sand shoals, and the 'sink' will be calculated based on island area changes (Table S7).

Table S7. Data for source-to-sink calculation.

Source		reference
Calculation equation	Production rate × Sand shoal area	(*5*)
Production rate ($g \times m^{-2} \times yr^{-1}$)	Min: 7.9, Median: 165, Max: 2900	(*5*)
Sand Shoal area (m^2)	63×10^6 (Joulters Cays) 80×10^6 (Abacos)	This study
Sink		
Calculation equation	Changes in islands area × Changes in elevation × (1- Porosity) × Density	(*6*)
Changes in islands area (m^2)	2280000 (Joulters Cays) 1440000 (Abacos)	This study
Changes in elevation (m)	Min: 0.5, Max: 1.5	TCarta DEM
Porosity	30%	(*5*)
Density (kg/m^3)	2700	Density of calcite

Calculation of source

The production rate of ooid sands ranges from 7.9 to 2900 $g \times m^{-2} \times yr^{-1}$, with a median of 165 $g \times m^{-2} \times yr^{-1}$(*5*), and if assume all of them are coming from nearby sand shoals (size: 63 km^2 in vintage interpretation, the Joulters Cays) and all part of the sand shoals are active (i.e., able to produce ooids), we could work out that the shoals produced 4×10^4 to 1.5×10^7 t (median: 8.3×10^5 t) by using equation 6. In the North Abacos, the active sand shoals have a coverage of ~80 km^2 and were able to produce 0.5×10^6 t to 1.8×10^7 t (median: 1.04×10^6 t) of oolitic sand over 8 decades.

Calculation of sink

Based on the DEM, the near-island sand shoals have elevation between -0.2 m to 0.8 m. By assuming to maintain land plants on islands needs elevation of 1.3 m, we can work out the changes in elevation is between 0.5 and 1.5 m. At the Joulters Cays, the islands have grown by 2.28km^2, by assuming the porosity of 30% and density of 2.7 g/cm^3, and apply equation 5, the Joulters Cays islands may have received 1.11 to 3.32×10^6 t (mean: 2.21×10^6 t) of carbonate sediments in the last 80 years. Similarly, the North Abacos experienced 1.44 km^2 of land, which equals 0.57 to 1.68×10^6 t of carbonate sand.

Based on the rough calculation, we found that a substantial part of the ooid sand is pushed to above sea-level area. For the median production rate ($165 \ g \times m^{-2} \times yr^{-1}$) scenario, the produced ooids would not sufficient for island growth and other sediment sources, such as seagrass meadows or coral reefs, would be needed. Even for the maximum production rate scenario (the Joulters Cays: 1.5×10^7 t, the North Abacos: 1.8×10^7 t), 10% of ooids are accumulated on islands (the Joulters Cays: 3.32×10^6 t, the North Abacos: 1.68×10^6 t).

The large proportion of sand deposited in both regions suggest the relative importance of onshore transport in shallow marine sediments, and sluggish vertical sand accumulation. Such effect might be

related either to on-shore wave transport or recurring storms/hurricanes events (*2*). This may explain why there is significant gap between the short-term sediment accumulation rate and long-term accumulation rate from a 1D sediment log (i.e., Sadler effect (*15*)): in the short-term the accumulation is determined by production (production-limited accumulation). At longer timescales, the produced sediments would be redistributed to other places (if the accommodation space is sufficient) and the effective accumulation rate would 'decrease', as observed in a 1D column of sediment core. Therefore, such a 'smearing effect' would not only make the long-term accumulation rate significantly lower than the short-term accumulation rate, but also spatially redistribute and mix produced facies, making less facies alternating vertically in stratigraphy. This sediment budget calculation suggests that the presence of transport beyond habitat boundaries could result in a low-pass filtering effect of stratigraphy.

References:

1. C. Lopez-Gamundi, B. B. Barnes, A. C. Bakker, P. Harris, G. P. Eberli, S. J. Purkis, Spatial, seasonal and climatic drivers of suspended sediment atop Great Bahama Bank. *Sedimentology* **71**, 769–792 (2024).
2. P. Harris, J. Carlos Laya, M. Frazer, in *Second International Meeting for Applied Geoscience & Energy*. (Society of Exploration Geophysicists and American Association of Petroleum …, 2022), pp. 347–350.
3. R. Major, D. G. Bebout, P. M. Harris, Modern Carbonate Sediment Facies Heterogeneity at the Development Scale—An Example from Joulters Cays, Bahamas. (1997).
4. R. P. Major, D. G. Bebout, P. M. Harris, Recent evolution of a Bahamian ooid shoal: Effects of Hurricane Andrew. *GSA Bulletin* **108**, 168–180 (1996).
5. C. Lopez-Gamundi, B. B. Barnes, C. Betzler, P. M. Harris, A. M. Oehlert, G. P. Eberli, S. J. Purkis, The sediment budget of Great Bahama Bank—Earth's largest modern carbonate platform. *Geology*, (2025).
6. C. Lopez-Gamundi, T. Dobbelaere, E. Hanert, P. M. Harris, G. Eberli, S. J. Purkis, Simulating sedimentation on the Great Bahama Bank – Sources, sinks and storms. *Sedimentology* **69**, 2693–2714 (2022).
7. R. M. Hulshoff, Landscape indices describing a Dutch landscape. *Landscape Ecology* **10**, 101–111 (1995).
8. K. McGarigal, S. A. Cushman, M. C. Neel, E. Ene, FRAGSTATS: spatial pattern analysis program for categorical maps. *Computer software program produced by the authors at the University of Massachusetts, Amherst* **3**, (2002).
9. C. Murcia, Edge effects in fragmented forests: implications for conservation. *Trends in Ecology & Evolution* **10**, 58–62 (1995).
10. C. N. Drummond, P. J. Dugan, Self-organizing models of shallow-water carbonate accumulation. *Journal of Sedimentary Research* **69**, 939–946 (1999).
11. A. E. Stears, P. B. Adler, S. E. Albeke, D. H. Atkins, J. Studyvin, D. C. Laughlin, plantTracker: An R package to translate maps of plant occurrence into demographic data. *Methods in Ecology and Evolution* **13**, 2129–2137 (2022).
12. E. C. Geyman, A. C. Maloof, B. Dyer, How is sea level change encoded in carbonate stratigraphy? *Earth and Planetary Science Letters* **560**, 116790 (2021).
13. E. A. Fulton, A. D. M. Smith, C. R. Johnson, Effects of spatial resolution on the performance and interpretation of marine ecosystem models. *Ecological Modelling* **176**, 27–42 (2004).
14. M. Wu, P. M. Harris, G. Eberli, S. J. Purkis, Sea-level, storms, and sedimentation–Controls on the architecture of the Andros tidal flats (Great Bahama Bank). *Sedimentary Geology* **420**, 105932 (2021).
15. P. M. Sadler, Sediment accumulation rates and the completeness of stratigraphic sections. *The Journal of Geology* **89**, 569–584 (1981).